J. Fluid Mech. (2002), *vol.* 460, *pp.* 381–409.
DOI: 10.1017/S0022112002008340 Printed in the United Kingdom

Spreading and peeling dynamics in a model of cell adhesion

By S. R. HODGES[1] AND O. E. JENSEN[2]

[1]Department of Applied Mathematics and Theoretical Physics, University of Cambridge, Silver Street, Cambridge CB3 9EW, UK

[2]Division of Applied Mathematics, School of Mathematical Sciences, University of Nottingham, University Park, Nottingham NG7 2RD, UK

(Received 11 June 2001 and in revised form 13 December 2001)

To understand how viscous and elastic membrane forces mediate the adhesion of fluid-borne cells to biological surfaces under the action of specific receptor–ligand bonds, we consider a model problem in which a two-dimensional cell interacts with a plane adhesive surface. The cell is modelled as an extensible membrane under tension containing fluid of constant volume. Assuming rapid binding kinetics, molecular binding forces are described through a contact potential that is long-range attractive but short-range repulsive. Using lubrication theory to describe the thin-film flow between the cell and the plane, we model sedimentation of the cell onto the plane under adhesive forces, followed by removal of the cell from the plane under the action of an external force. Numerical simulations show how these events are dominated respectively by quasi-steady spreading and peeling motions, which we capture using an asymptotic analysis. The analysis is extended to model a cell tank-treading over an adhesive wall in an external shear flow. The relation between cell rolling speed and shear rate is determined: at low speeds it is linear and independent of the viscosity of the suspending fluid; at higher speeds it is nonlinear and viscosity-dependent.

1. Introduction

Cell adhesion is a process that occurs widely in the body. In blood vessels, for example, neutrophils bind to the walls of post-capillary venules in response to infection or injury as part of the inflammatory response, cancer cells bind to endothelium in metastasis, and platelets and monocytes adhere to atherosclerotic plaques. Understanding and controlling cell adhesion is therefore important in treating a range of significant diseases, and in manipulating the body's response to implants. The binding of a cell to an adhesive surface occurs through the action of specific intermolecular forces: receptor molecules on the surface of the cell membrane bind to complementary ligand molecules on the substrate. The resulting adhesive forces compete with other mechanical stresses (such as elastic forces in the cell membrane and viscous forces in the suspending fluid) in determining whether or not the cell adheres to the surface. Reviews of some of the extensive literature on cell adhesion can be found in Lauffenburger & Linderman (1993), Springer (1995), Hammer & Tirrell (1996), Jones, Smith & McIntyre (1996), Zhu (2000) and Orsello, Lauffenburger & Hammer (2001).

The binding of neutrophils to endothelium, in particular, has been extensively investigated, and is now understood to occur as a multi-step process (see for example

Lawrence & Springer 1991). Initially selectin receptors and their carbohydrate ligands, which can bind to one another rapidly and reversibly, capture the neutrophil from the blood stream and lead to 'rolling', in which the cell wanders slowly (at speeds substantially less than that of the free stream) but erratically over the endothelium (Atherton & Born 1973; Goetz *et al.* 1994; Lawrence 1999). Here small numbers of receptors on the tips of microvilli (short protrusions of the cell membrane) bind transiently to the vessel wall, so that at any instant the cell pivots around a small number of individual bonds. Rolling allows the cell to survey the endothelium for signs of inflammation. Chemoattractants released from a site of injury activate integrin receptors on a rolling neutrophil, which bind to immunoglobulin ligands on endothelial cells, leading to firmer adhesion and bringing the cell to rest. The neutrophil then flattens against the endothelium before migrating between endothelial cells towards its target site.

Theoretical modelling of the adhesion of fluid-borne cells to adhesive surfaces presents significant challenges. These concern, for example, the nature of the intermolecular bonds, the mechanical properties of the membranes and surfaces in which binding molecules sit, and the mechanical properties of the whole cell and its fluid environment. We review these topics briefly before addressing below the hydrodynamical issues that are the subject of this paper.

Bond formation and breakage is a statistical process that can be modelled as a reversible chemical reaction between populations of free and bound bonds. The reaction is characterized by forward and reverse reaction rates. An external force F applied to a bond will alter these reaction rates, typically increasing the rate of bond breakage K_r. Such effects have been modelled in a number of different ways. Bell (1978) proposed the phenomenological relationship $K_r \propto \exp(\sigma F/k_B T)$, where σ is a lengthscale in the bond's energy landscape and $k_B T$ one unit of thermal energy. A closely related model was proposed by Dembo *et al.* (1988), who treated bonds as stretched springs and assumed K_r depends on the energy in the bond (see (2.2) below). More recent models account for the rate at which the force is applied to the bond (e.g. Evans & Ritchie 1997). Currently a range of experimental techniques (such as atomic force microscopy, the surface force apparatus, the biomembrane force probe and optical tweezers) are being used to probe the effects of applied forces on bond strength (e.g. Bongrand 1999; Leckband 2000). Kinetic rate constants and equilibrium constants have been measured in cell systems (e.g. Alon *et al.* 1998; Smith, Berg & Lawrence 1999; Piper, Swerlick & Zhu 2000), with recent studies supporting the use of Bell's (1978) model in describing selectin bonds, for example (Chen & Springer 2001).

The competition between adhesive forces and elastic stresses in a cell membrane was described by Evans (1985), who computed local, static shapes of a membrane (modelled as a beam with bending stiffness) in the neighbourhood of an adhesive surface; the shape of complete vesicles subject to an adhesive potential at a wall has since been computed by, for example, Seifert & Lipowsky (1990) and Seifert (1991). Dembo *et al.* (1988) extended Evans' tape-peeling analysis by introducing the spring-based bond model described above, determining the equilibrium contact angle of a statically adhered membrane under given tension, and then showing how bond kinetics control dynamic spreading and peeling speeds when the peeling angle (or tension) is either greater than, or less than, its equilibrium value. Various extensions of this model have been proposed to account for the effects of non-specific forces, clustering of adhesion receptors (Ward & Hammer 1993) and limited ligand density (Ward, Dembo & Hammer 1995).

Hammer & Lauffenburger (1987) introduced hydrodynamics to the problem of cell adhesion by exploiting classical solutions (Goldman, Cox & Brenner 1967*a*, *b*) for the force and torque on a smooth rigid sphere rolling in a shear flow over a flat plane at zero Reynolds number. They balanced hydrodynamic forces on the cell with adhesive forces arising from distributed bonds in a small region at the base of the cell, close to the plane, employing Bell's (1978) kinetic model, to determine the number and strength of receptors required for adhesion. Since only a few bonds are involved in neutrophil rolling, Hammer & Apte (1992) subsequently introduced 'adhesive dynamics' simulations. Here a rigid sphere is coated with a distribution of adhesive springs: each spring represents a microvillus with a receptor molecule at its tip. The sphere moves close to the wall, with transient binding occurring between a few springs and the wall. The motion of the sphere is computed by balancing hydrodynamic forces and torques (computed using the results of Goldman *et al.* 1967*a*, *b*) with those arising from a few adhesive contacts. (A similar approach was also taken by Tözeren & Ley 1992.) The Monte Carlo simulations used in adhesive dynamics provide a natural means for studying the stochastic nature of neutrophil rolling. Recent simulations support the use of Bell's (1978) model for a wide class of receptor–ligand pairs (Chang, Tees & Hammer 2000), and boundary-element techniques have been exploited to describe cell–cell interactions (King & Hammer 2001). Alternative stochastic models for binding kinetics and transient cell adhesion have also been developed (e.g. Zhu 2000; Zhu, Bao & Wang 2000).

A recent refinement of the microvillus-covered-sphere model of neutrophil rolling was presented by Zhao, Chien & Weinbaum (2001), who included the effects of weak gravity, causing the cell to sediment slowly onto the endothelium. Zhao *et al.* suggest that this very weak body force combined with a strong shear flow can lead to large but short-lived contact forces between microvilli tips and the wall, sufficient for the tips to penetrate the glycocalyx (the layer of charged glycoproteins) coating endothelial cells. This model is used to explain the shear threshold required for L-selectin-mediated binding seen experimentally (Finger *et al.* 1996), although alternative mechanisms have also been proposed (e.g. Chen & Springer 1999; Chang & Hammer 1999).

Despite the success of adhesive dynamics simulations and related studies, it is important to recognize that adhering cells such as leukocytes do not always have the hydrodynamical properties of smooth rigid spheres (Tissot *et al.* 1992; Damiano *et al.* 1996). For example, Wu *et al.* (1998) demonstrated using integrin-mediated adhesion of epithelial cells to laminin that increased cell deformability reduces mean rolling speeds. Sheikh & Nash (1998) also showed how adhesion properties of leukocytes are altered if cytoskeletal structures are disrupted. Such observations have motivated computational studies of flows over adhered cells with non-spherical shapes (e.g. Olivier & Truskey 1993; Brooks & Tözeren 1996; Gaver & Kute 1998). Others have computed shear flows over deformable model cells statically adhering to an interface (Kan *et al.* 1999): here studies of flows over liquid drops adhering to plane surfaces are relevant (e.g. Dussan V. 1987; Feng & Basaran 1994; Li & Pozrikidis 1996; Dimitrakopoulos & Higdon 1997; Schleizer & Bonnecaze 1999). These studies demonstrate how static drops (and cells) require a difference between their front and rear contact angles to balance the viscous forces due to the oncoming shear flow, provided viscous forces (measured relative to surface tension forces by a capillary number) are small enough for a steady drop configuration to be possible.

There have been only a few computational studies of deformable drops or cells rolling or sliding over adhesive surfaces. Schleizer & Bonnecaze (1999) introduced slip at an adherent drop's contact lines, and showed how a steady sliding motion

is possible provided the capillary number is not too great. Lei, Lawrence & Dong (1999) used CFD methods to determine the rolling speed of a two-dimensional cell (modelled as a membrane under tension containing viscous fluid) in a planar channel, where the cell binds to one channel wall with adhesive bonds governed by kinetics of the kind proposed by Dembo *et al.* (1988). The speed of rolling was determined by an energy dissipation argument. Their results showed that despite a high cytoplasmic viscosity, the majority of viscous dissipation occurs in the fluid outside the cell, although increased cytoplasmic viscosities could reduce rolling speeds significantly. In a related computational study, Dong *et al.* (1999) highlighted the role of the small 'peeling' zone at a rolling cell's trailing edge in controlling cell rolling speeds. Other studies (Cantat & Misbah 1999; Seifert 1999; Sukumaran & Seifert 2001) of Stokes flows over deformable drops or vesicles adhering to a wall have demonstrated that viscous effects can give rise to a lift force arising from large lubrication pressures in the thin film beneath the vesicle and the wall, which can be sufficient to completely lift the vesicle off the wall.

The aim of the present study is to use a deterministic, continuum model to explore the competition between specific binding forces, cell membrane stresses and viscous forces in the adhesion of a cell to a plane wall. In contrast to previous computational studies (e.g. Lei *et al.* 1999; Dong *et al.* 1999; Dong & Lei 2000), we exploit asymptotic methods as far as possible to understand how a cell spreads over, peels away from, or rolls over an adhesive surface. In particular, we use lubrication theory to describe the flow in the thin liquid film between the cell and the wall, and consider parameter regimes in which the flows in this region control the motion of the whole cell. To keep the model tractable, we restrict attention to a two-dimensional geometry, and model the cell as a thin membrane under tension containing incompressible fluid having viscosity low enough that it can be treated as inviscid. We model binding kinetics following Dembo *et al.* (1988), but to highlight hydrodynamic effects we assume bond formation and breakage occur rapidly compared to flow timescales. The model then has the attractive feature that the bonds can be represented by an adhesive potential that is long-range attractive but short-range repulsive. Our results therefore share common ground with studies of thin liquid layers which rupture or spread under the influence of long-range intermolecular forces (e.g. Williams & Davis 1982; Mitlin 1993; Sharma & Jameel 1993; Oron 2000; Eres, Schwartz & Roy 2000). This idealized model does not seek to model a specific cell system (such as rolling neutrophils): our aim instead is to highlight hydrodynamic mechanisms that may be important in a range of applications in cell adhesion and, more generally, colloidal aggregation.

After describing the model (§ 2), we consider three closely related problems. First (§ 3), we treat a freely suspended cell that moves normally towards a wall under the action of adhesive forces (which we call 'sedimentation,' although gravitational effects are neglected here). As binding forces deform the cell membrane, it spreads over the wall at a rate that is limited (in this model) by viscous dissipation in the suspending fluid. We use thin-film asymptotics to predict spreading rates. Second (§ 4), we suppose an external force is applied to a bound cell, lifting it upwards off the wall (simulating micropipette aspiration (Hochmuth 2000)). Once again, hydrodynamic pressures in the suspending fluid contribute to the dynamic adhesive force and influence the rate at which the membrane peels of the wall. The dynamic shape assumed by the membrane as it binds to the wall is quite distinct from that which arises as the cell is pulled off the wall. Finally (§ 5), we consider a cell that is adhered to a wall but which is also subject to an external shear flow. The cell tank-treads over the wall, spreading at its front and peeling at its rear at a rate limited by viscous dissipation in the fluid

outside the cell; we use asymptotic approximations to obtain a prediction for the rolling speed as a function of the imposed shear rate, the strength and nature of the binding forces, and the membrane tension.

2. The model

In this section we derive the evolution equation and associated boundary conditions ((2.14), (2.15), below) used to describe the sedimentation of a cell onto, or aspiration from, an adhesive plane wall. We first describe the model for the intermolecular bonds (§ 2.1) and their effect on static cell configurations (§§ 2.2, 2.3), and then explain briefly how lubrication theory can be used to model the flow of the thin liquid layer between the cell and the wall (§ 2.4).

2.1. *Adhesion bonds*

Our model for the bonds between a cell membrane and an adjacent plane wall follows closely that proposed by Dembo *et al.* (1988), so only a brief summary is given here. We suppose ligand molecules are uniformly and densely distributed on the substrate, and receptor molecules are uniformly distributed on the cell membrane with density A_{tot} bonds per unit area. We suppose a bound receptor–ligand pair behaves like a simple Hookean spring with undisturbed length λ and spring constant κ. The bonds are stretched normally from the wall to the cell membrane, supplying a vertical force on the cell. While this assumption may be unrealistic in general, it is a reasonable first approximation when the membrane slope in the region of bond formation is small.

We assume that the formation and breakage of adhesion bonds is a reversible chemical process of the type $A_f \rightleftharpoons A_b$, where A_f is the density of free adhesion molecules on the membrane, A_b is the density of consummated bonds and $A_{tot} = A_f + A_b$. The forward and reverse reaction rates are K_f and K_r, each of which is assumed to be a function of the cell-to-surface gap $H^\star$ measured normally from the wall.

Provided reaction rates are rapid relative to the timescale of any flows, so that the bond distributions are always in equilibrium, then $A_f K_f = A_b K_r$, so that

$$A_b(H^\star) = \frac{A_{tot} K_f(H^\star)/K_r(H^\star)}{1 + [K_f(H^\star)/K_r(H^\star)]}. \tag{2.1}$$

It is then assumed that the relative chance of a bond forming or breaking depends on the energy E held within that bond via a Boltzmann distribution, so that the association constant is

$$\frac{K_f(H^\star)}{K_r(H^\star)} = \exp\left(-\frac{E}{k_B T}\right), \tag{2.2}$$

where k_B is the Boltzmann constant and T the absolute temperature. Treating each bond as a spring, $E(H^\star) = E_0 + \frac{1}{2}\kappa(H^\star - \lambda)^2$ where E_0 is the energy held within an undisturbed bond. Writing $K_{eq} = K_f(\lambda)/K_r(\lambda)$, (2.1) and (2.2) give, for $K_{eq} \ll 1$,

$$A_b(H^\star) = A_{tot}\, K_{eq} \exp\left(-\frac{\kappa}{2k_B T}(H^\star - \lambda)^2\right). \tag{2.3}$$

The assumption of low binding affinity $K_{eq} \ll 1$ is made here only in order to simplify the model while retaining its most important qualitative features, and is easily relaxed.

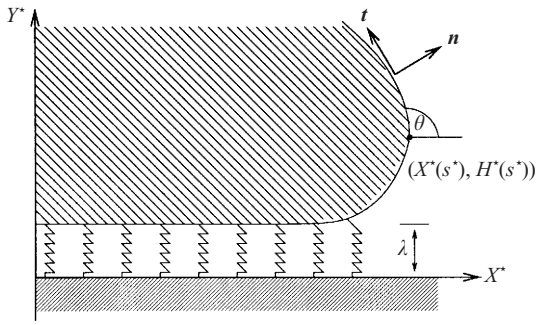

FIGURE 1. Schematic illustration of a static cell bonded to a plane wall by adhesion molecules of equilibrium length λ. Each point of the cell boundary $(X^\star, H^\star)$ is parameterized by the dimensional arc length $s^\star$.

2.2. *Cell mechanics*

We model a cell as a thin, two-dimensional, extensible membrane subject to tension but having negligible bending stiffness, surrounding a fluid interior of fixed volume per unit length. The viscosity of the cell's interior is assumed to be low enough that it behaves as if it were inviscid. When undisturbed, the cell is circular with radius R; it deforms under the action of adhesive forces. The effects of gravity and non-specific forces acting on the cell are neglected. We define $X^\star(s^\star)$ and $Y^\star = H^\star(s^\star)$ to be the (dimensional) Cartesian coordinates of the cell membrane with respect to the wall, $s^\star$ the arc length along the membrane, $p^\star$ the pressure in the fluid outside the cell and $P_c^\star$ the pressure inside the cell, as illustrated in figure 1. The stress balance on the membrane when the cell and fluid are in static equilibrium is then (Dembo *et al.* 1988)

$$A_b(H^\star)\kappa(H^\star - \lambda)(X^\star_{s^\star}\boldsymbol{n} - H^\star_{s^\star}\boldsymbol{t}) + (P_c^\star - p^\star)\boldsymbol{n} = C^\star T^\star \boldsymbol{n} - T^\star_{s^\star}\boldsymbol{t}. \tag{2.4}$$

Here vertical bonds, acting as springs, and the transmembrane pressure difference, are balanced by the tension T^* in the cell membrane. Subscripts $s^\star$ denote derivatives, $C^\star$ is the membrane curvature and $\boldsymbol{n}$ and $\boldsymbol{t}$ are normal and tangential unit vectors. We non-dimensionalize by scaling lengths on R (so that $H^\star = RH$, etc.), tension on a reference tension τ and pressures on τ/R. Equations (2.3) and (2.4) then give, in the normal and tangential directions,

$$CT = \frac{M(H-\epsilon)}{\epsilon \exp\left(\dfrac{\gamma}{2\epsilon^2}(H-\epsilon)^2\right)}\cos\theta + P_c - p, \quad T_s = \frac{M(H-\epsilon)}{\epsilon \exp\left(\dfrac{\gamma}{2\epsilon^2}(H-\epsilon)^2\right)}\sin\theta, \tag{2.5a,b}$$

where

$$X_s = \cos\theta, \quad H_s = \sin\theta, \quad C = \theta_s. \tag{2.6}$$

Static cell shapes are then parameterized by

$$\epsilon = \frac{\lambda}{R}, \quad M = \frac{\kappa A_{tot} K_{eq} R^2 \epsilon}{\tau}, \quad \gamma = \frac{\kappa\lambda^2}{kT}. \tag{2.7}$$

Here ϵ represents the length of the adhesion molecules relative to the size of the cell, M represents the total adhesive force of the adhesion molecules relative to the cell membrane tension and γ relates the energy of a bond to thermal energy fluctuations.

Neutrophils provide a well-studied system from which we can estimate typical parameter values. The P-selectin molecule extends about 40 nm from the endothelial cell membrane, so when combined with its ligand PSGL-1 it is reasonable to take

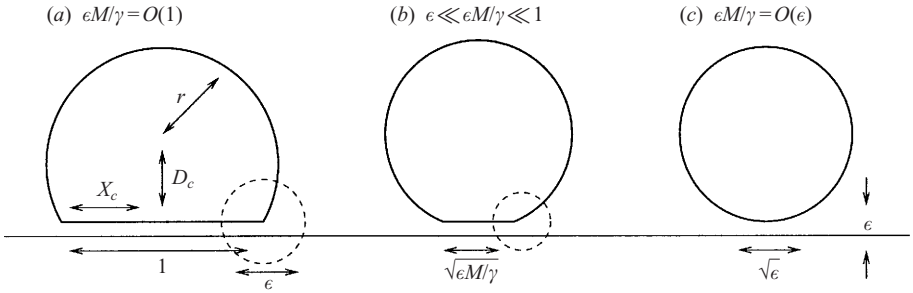

FIGURE 2. Schematic diagram of the three regimes of static adhesion, showing typical lengthscales of asymptotic regions.

$\lambda \approx 100\,\text{nm}$ as an estimate of the length of the unstressed bond. This is of similar magnitude to the static length of a microvillus (0.3 μm, Shao, Ting-Beall & Hochmuth 1998). Taking $R \approx 4\,\mu\text{m}$ gives $\epsilon \approx 0.025$. A P-selectin/PSGL-1 bond is formed in series with a more extensible microvillus, with stiffness $\kappa \approx 0.04\,\text{g s}^{-2}$ (Shao *et al.* 1998). Membrane tension is $\tau \approx 0.024\,\text{g s}^{-2}$ (Hochmuth 2000), and $A_{tot} = 20\,\mu\text{m}^{-2}$ is comparable to values used in Smith *et al.* (1999). This gives $M \approx 13K_{eq}$. Direct measurements of K_{eq} are scarce, but values in the hundreds have been used in previous models (e.g. King & Hammer 2001). With $k_B T \approx 4 \times 10^{-14}\,\text{g cm}^2\,\text{s}^{-1}$, $\gamma \sim 100$. There may of course be considerable variation in these parameters between different cell systems. In simulations below we take $M = 100$, $\gamma = 1$ and assume $\epsilon \ll 1$; asymptotic results will confirm that these simulations are representative of a broad range of parameter values.

2.3. *Static cell shapes*

In static equilibrium, we impose symmetry about $X = 0$, and take $p = 0$; P_c must be chosen so that the cell's dimensionless area remains equal to π. Equations (2.5), (2.6) can then be solved to give the shape of a static cell bound to a wall. Here we briefly consider an asymptotic solution of this problem, assuming $\epsilon \ll 1$. We split the cell into two distinct regions: an outer region, an $O(1)$ distance from the wall, where adhesion forces are negligible in (2.5); and an inner region adjacent to the wall, where $H = O(\epsilon)$ and the spring terms in (2.5) are significant. In the outer region, in the absence of any other external forces, the cell has uniform tension and uniform curvature. It is convenient to define τ to be the dimensional tension of the cell in this region, so that here the membrane is circular and $T = 1$.

Where the cell is close to the wall (the inner region), we write $H(X) = \epsilon h(X)$ so that (2.5*a*, *b*) can be combined to give

$$\left(1 - \frac{\epsilon M/\gamma}{\exp(\frac{1}{2}\gamma(h-1)^2)}\right) \frac{\epsilon h_{XX}}{(1+(\epsilon h_X)^2)^{3/2}} = \frac{M(h-1)}{\exp(\frac{1}{2}\gamma(h-1)^2)\sqrt{1+(\epsilon h_X)^2}} + P_c. \quad (2.8)$$

Solutions of (2.8) must be matched to the circular membrane in the outer region. Three distinct parameter regimes emerge, illustrated in figure 2.

For $\epsilon M/\gamma = O(1)$, the cell membrane is flat with $h = 1$ along the majority of the inner region, which has $O(1)$ length, but it has sharp corners where it connects to the outer solution at $X = \pm X_c$, say. Assuming cell membrane gradients are $O(1)$ at the corner, we write $X = X_c + \epsilon x$, and discard the $O(\epsilon)$ pressure term in (2.8). The

resulting equation can be integrated exactly (Dembo *et al.* 1988), giving

$$h_x = H_X \to \left(\frac{1}{(1-\epsilon M/\gamma)^2} - 1 \right)^{1/2} \quad \text{as} \quad x \to \infty, \tag{2.9}$$

which provides the effective equilibrium contact angle where the membrane meets the wall. A geometrical argument then yields the radius of the circular part of the cell r, the cell's internal pressure $P_c = r^{-1}$, the vertical distance of the cell centre from the wall D_c and the contact length of the bottom of the cell with the wall $2X_c$, where

$$\begin{aligned} &r = \pi^{1/2}(\pi - \tan^{-1}\Omega + (1-\epsilon M/\gamma)^2\Omega)^{-1/2}, \\ &\Omega D_c = X_c = (1-\epsilon M/\gamma)\Omega r, \quad \Omega = ((1-\epsilon M/\gamma)^{-2} - 1)^{1/2}. \end{aligned} \tag{2.10}$$

The cell shape in the outer region depends only on the ratio $\epsilon M/\gamma$. The limit $\epsilon M/\gamma \to 1$ represents the limit of maximum adhesion, in which the outer solution is semicircular. The present model is not self-consistent for $\epsilon M/\gamma > 1$.

Reducing $\epsilon M/\gamma$ corresponds to reducing the strength of adhesion molecules or making the cell less deformable. If $\epsilon M/\gamma = O(\epsilon)$, there is a single inner region of length $O(\epsilon^{1/2})$ (figure 2*c*). We focus in this paper on the intermediate case, for which $\epsilon \ll \epsilon M/\gamma \ll 1$ (figure 2*b*). Here the half-length of the bound portion of the cell membrane and the effective contact angle in the corner region both shrink to $(2\epsilon M/\gamma)^{1/2} + O((\epsilon M/\gamma)^{3/2})$, but the corners remain distinct from the uniform region between them. This limit will allow us to use lubrication theory to describe the flow of liquid between the cell and the wall, while also exploiting the asymptotic separation of scales between the film and corner regions. In this limit $r = P_c = 1 + O((\epsilon M/\gamma)^{3/2})$; since the cell membrane is not significantly stretched from its original circular shape, τ is effectively the tension of the cell when undeformed.

The model presented so far describes a static cell bound to an adhesive wall. A bound cell may be removed from the wall experimentally by micropipette aspiration. We model an aspirated cell by applying a vertical force per unit length $2k\epsilon^{1/2}$ to the top-most point of the cell, where $s = s_0$, say. This is represented by adding a term $2k\epsilon^{1/2}\delta(s - s_0)$ to (2.5*a*). Then, for $\epsilon \ll \epsilon M/\gamma \ll 1$, the outer solution is now two arcs of circles meeting at $s = s_0$, each subtending an angle $k\epsilon^{1/2}$ to the horizontal at $s = s_0$ to satisfy a local vertical force balance. r, P_c, D_c and X_c must also be modified from the values given in (2.10); in particular,

$$X_c = \epsilon^{1/2}((2M/\gamma)^{1/2} - k) + O((\epsilon M/\gamma)^{3/2}), \tag{2.11}$$

$$D_c = 1 + (2k\epsilon^{1/2}/\pi) - (25k^2\epsilon/(4\pi)) - (\epsilon M/\gamma) + O((\epsilon M/\gamma)^{3/2}), \tag{2.12}$$

so that if $k > (2M/\gamma)^{1/2}$ the cell will be completely removed from the wall.

2.4. *Cell and fluid dynamics*

We use lubrication theory (Oron, Davis & Bankoff 1997) to describe transient flows in the thin gap between the cell and the wall, where now h is a function of x and time t. We formulate the problem in the point-contact regime (figure 2*c*) by scaling $Y = \epsilon y$, $X = \epsilon^{1/2}x$; this formulation incorporates as a special case the limit $\epsilon \ll \epsilon M/\gamma \ll 1$. Since the fluid layer is thin, the pressure p in the fluid film beneath the cell is non-uniform but independent of y (to leading order in ϵ). Pressure gradients in the film drive a fluid flux, which is resisted by viscous forces. To keep the model simple, we assume fluid motions can be characterized by a constant viscosity μ; it is likely that surface structures such as glycocalyx or membrane roughness would significantly

alter the permeability of the gap between the cell and the wall (see, for example, Feng & Weinbaum 2000), but we do not account for such effects explicitly here. With horizontal velocities scaled on $\tau\epsilon^{3/2}/\mu$, vertical velocities on $\tau\epsilon^2/\mu$ and time on $R\mu/\epsilon\tau$, the viscous contribution to the normal stress is $O(\epsilon)$ smaller than the pressure, and variations in tension due to viscous tangential stress are $O(\epsilon)$ smaller than the mean value of the tension τ, so neither effect enters (2.5), (2.6). Thus the normal stress condition becomes

$$p(x,t) = 1 + \frac{M(h-1)}{\exp(\frac{1}{2}\gamma(h-1)^2)} - h_{xx} + O(\epsilon, \epsilon M/\gamma). \tag{2.13}$$

The three contributions in (2.13) arise respectively from the pressure in the cell, the effects of binding forces (which are equivalent to a conjoining/disjoining pressure which represents a force that is long-range attractive but short-range repulsive), and membrane tension. We impose $p \to 0$ as $x \to \pm\infty$, to match with the external fluid pressure far from the thin-film region.

The horizontal fluid flux under the cell is $Q = -p_x h^3/12$; the effects of inertia can be neglected provided $\rho\tau\epsilon^3 R/\mu^2 \ll 1$, where ρ is the density of the liquid. Combined with (2.13) and the mass conservation equation $h_t + Q_x = 0$, we obtain a dimensionless evolution equation for the thickness of the liquid film beneath the cell,

$$h_t - \frac{1}{12}\left[h^3\left(\frac{M(h-1)}{\exp(\frac{1}{2}\gamma(h-1)^2)} - h_{xx}\right)_x\right]_x = 0, \tag{2.14}$$

which is solved subject to boundary conditions

$$h_x(0,t) = h_{xxx}(0,t) = 0, \quad h \to \tfrac{1}{2}x^2 + kx + \beta(t) \quad \text{as} \quad x \to \infty. \tag{2.15a,b}$$

Equation (2.15a) ensures symmetry about $x = 0$, which is appropriate for the sedimentation and aspiration problems considered below; (2.15b) allows matching with the circular outer solution. The function $\beta(t)$ must be determined as part of the solution; it measures the vertical displacement of the cell centre, which lies at $X = 0$, $Y = D_c = 1 + \epsilon\beta$ when $k = 0$. When the cell is sedimenting to the wall under the action of adhesive forces alone the outer solution is perfectly circular and $k = 0$. Setting $k > 0$ models aspiration, when a vertical point force $2k\epsilon^{1/2}$ is applied to the top of the cell.

3. Sedimentation onto an adhesive wall

We present first solutions of (2.14), (2.15) with $k = 0$, modelling the sedimentation of a cell towards a plane wall under the action of adhesive intermolecular forces. We take $h(x,0) = \frac{1}{2}x^2 + \beta(0)$, where $\beta(0) = 5$, so that the cell is initially circular and a dimensional distance 5λ from the wall. Numerical solutions are presented in § 3.1: they were obtained by discretizing (2.14), (2.15) with finite differences in space and time-stepping using an implicit routine from the NAG library. An asymptotic description of the resulting quasi-steady spreading motions is presented in § 3.2.

3.1. *Numerical results*

Most of the solutions presented below used 1000 grid points over a domain of length 20. The accuracy of the results was checked by independently varying the number of grid points and the domain length.

Figure 3 shows $h(x,t)$ and $p(x,t)$ (defined in (2.13)) during sedimentation onto an

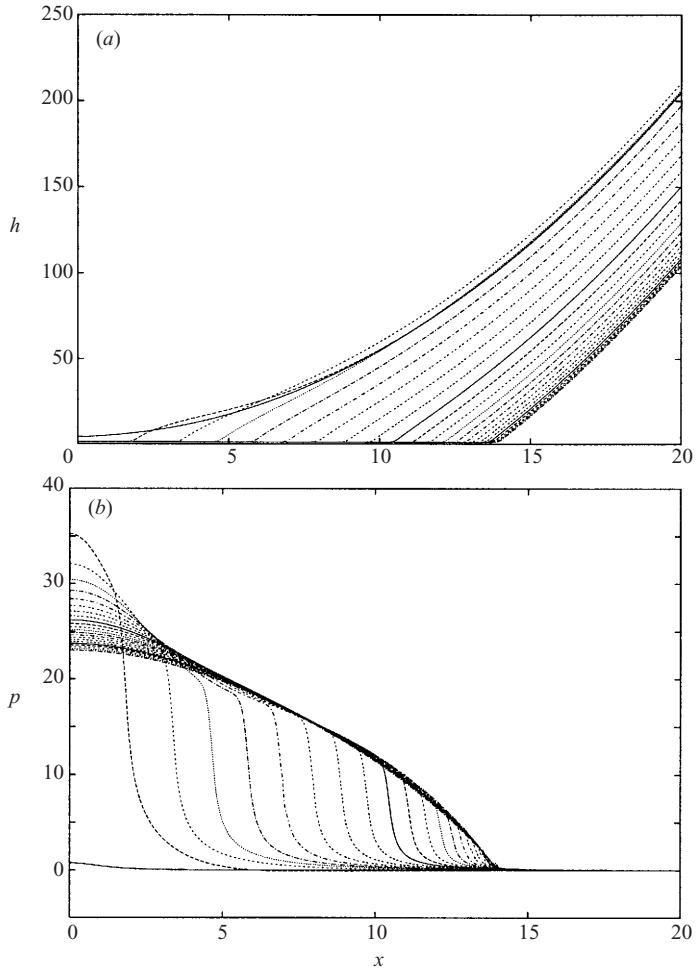

FIGURE 3. Solutions of (2.14), (2.15) with $k = 0$, $M = 100$, $\gamma = 1$ and $\beta(0) = 5$, showing a cell spreading onto an adhesive surface. Solutions are shown for $t = 1$ (solid) and at increasing time increments of 0.04. (*a*) Film thickness h versus x; near the wall, the cell membrane moves from left to right with time. (*b*) p versus x; the pressure wave moves from left to right.

adhesive wall for $M = 100$ and $\gamma = 1$. Figure 4(*a*) shows $\beta(t)$ and $x_{\min}(t)$ for the same simulation, where $x = x_{\min}$ (defined by $h_{\min} = h(x_{\min}, t)$) gives a good indication of the length of the portion of the cell membrane which is firmly attached to the wall. The rate at which the fluid layer thins is shown in figure 4(*b*), which plots $h(0, t)$ and $h_{\min}(t)$. We can identify four distinct phases of the adhesion process, marked (i)–(iv) in figure 4.

In the first phase, which we term *drifting*, the cell remains far enough away from the wall for the adhesion molecules to have little effect on the cell. The cell remains roughly circular and moves slowly towards the wall under the effect of very weak long-range forces (see $h(0, t) = h_{\min}(t)$ in figure 4*b*). This phase lasts until $t \approx 1$ in this simulation. The cell then enters the short *capture* phase, where the base of the cell is close enough to the wall for adhesive forces to become substantially stronger. The base of the cell is quickly pulled down and bonded to the wall (figure 4*b*, phase (ii)), which squeezes fluid sideways, forming pockets of trapped fluid at either side of the

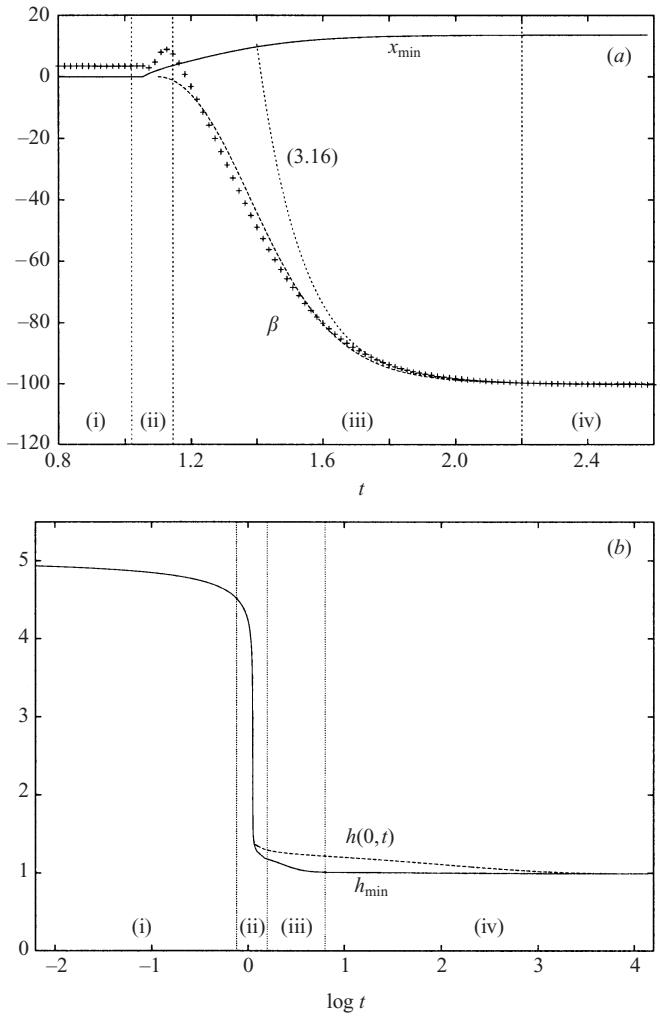

FIGURE 4. (*a*) Cell centre displacement $\beta(t)$ (symbols) and $x_{min}(t)$ (solid line). The dashed line shows the asymptotic estimate of $\beta(t)$ from (3.2), (3.24), (3.25); the dotted line shows (3.16). (*b*) $h_{\min}(t)$ (solid) and $h(0,t)$ (dashed), computed using (2.14), (2.15) for $M = 100$, $\gamma = 1$, $\beta(0) = 5$. (i)–(iv) correspond to *drifting, capture, spreading* and *draining* phases respectively.

cell base. This creates a distinct concave bulge in the cell membrane (e.g. $t = 1.04$, figure 3*a*). A disturbance is then transmitted in a whip-like fashion along the cell membrane to the outer edge of the flow domain. This is illustrated in figure 5, which shows x_D versus t, where $x_D(t)$ tracks the most right-hand maximum of $h - \frac{1}{2}x^2$, providing a measure of the position of the advancing disturbance.

We can see from figure 4 (phase (ii)), which shows a transient hump in $\beta(t)$ and a rapid fall in $h(0,t)$, that the primary effect of the sudden sideways displacement of fluid beneath the cell is, surprisingly, to lift the centre of the cell upwards during the brief capture phase. The way in which the whip-like disturbance spreads along the cell membrane, where the membrane is far enough from the wall for adhesion forces to be insignificant, can be understood by considering (2.14) without the spring term. Since $h \sim \frac{1}{2}x^2$ for large x, a balance between the first and third terms in (2.14) suggests

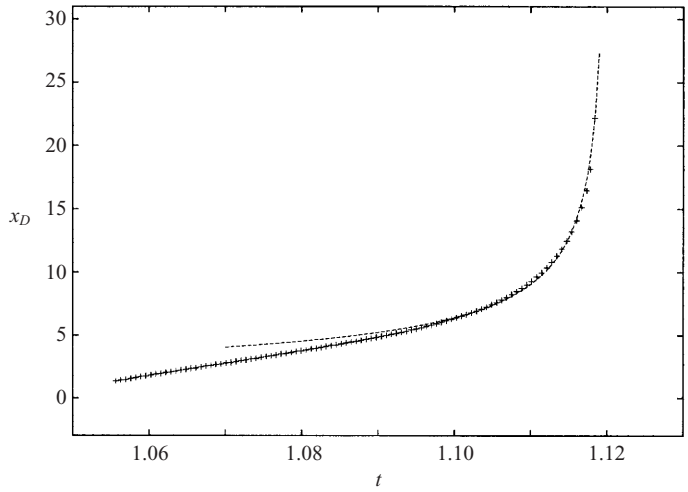

FIGURE 5. Symbols are numerical data for the disturbance's leading edge $x_D(t)$ during the capture phase for $M = 100$, $\gamma = 1$, $\beta(0) = 5$. The dashed line is $0.9(1.12 - t)^{-1/2}$.

that x_D scales like $(t_0 - t)^{-1/2}$ as $t \to t_0^-$, for some t_0. Numerical solutions in figure 5 are consistent with this scaling, with $t_0 \approx 1.12$ for these parameter values, indicating that the system exhibits a weak finite-time singularity. Computations suggest that the amplitude of the disturbance decays like $(t_0 - t)^2$, although we were unable to find a self-similar solution of (2.14) consistent with these observations.

After capture, the cell enters the longer quasi-steady *spreading* phase of cell adhesion ((iii) in figure 4). Here, the base of the cell spreads smoothly along the wall towards its final equilibrium configuration (figure 3*a*). The length of the bound portion of the cell membrane increases to its final static contact length $x_c = (2M/\gamma)^{1/2}$, in agreement with (2.11). The cell centre moves downwards towards the wall (figure 4*a*), with $\beta \to -M/\gamma$ as t increases so that $D_c \to 1 - \epsilon M/\gamma$, again in agreement with the static result (2.12). A travelling pressure wave (figure 3*b*), which is coincident with the membrane corner, advances towards $x = x_c$. The pressure in the film deposited behind the advancing membrane is large, indicating that the film is slightly thicker than the equilibrium thickness $h = 1$. The pressure (and film thickness) immediately behind the travelling wave decrease as the speed of the advancing corner reduces to zero, leaving a non-uniform pressure distribution at the end of the spreading phase. Early in spreading, when the corner is moving rapidly, the pressure in the fluid decays slowly to zero over a substantial distance ahead of the advancing corner. The elevated fluid pressure ahead of the corner creates a weak bulge in the membrane in this region.

Finally, once the membrane corner has reached its equilibrium position, fluid trapped beneath the cell is squeezed out by spring forces into the surrounding fluid, as illustrated in figure 4(*b*) (phase (iv)), where $h(0, t)$ falls slowly to $h = 1$ as t increases. We call this last stage the *draining* phase. The pressure in figure 3 is shown up to the end of the spreading phase; thereafter it falls to zero as t increases. The decay is governed approximately by the linear diffusion equation

$$h'_t = \frac{M}{12} h'_{xx}, \tag{3.1}$$

taking $h = 1 + h'$, $|h'| \ll 1$, $M \gg 1$ in (2.14). Since the trapped film has length $O(M^{1/2})$, draining occurs over $O(1)$ timescales (figure 4*b*).

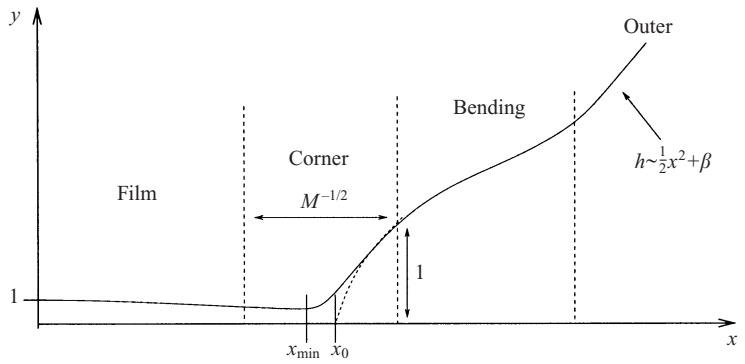

FIGURE 6. Schematic diagram of the asymptotic regions during the spreading phase of cell adhesion.

3.2. *Spreading asymptotics*

Figures 3 and 4(*a*) show that the spreading phase ((iii) in figure 4) dominates the adhesion process in sedimentation. Here we present an asymptotic analysis of the cell's motion during this phase, assuming $M \gg 1$ and $\gamma = O(1)$ in (2.14), (2.15), which provides explicit predictions of $\beta(t)$, for example, and which helps us understand the physical balances controlling the rate at which a cell spreads over an adhesive surface in a fluid environment.

We assume that the membrane exhibits a distinct corner that lies between $x = 0$ and $x = x_c$, but which is not too close to either extreme, and that the motion is quasi-steady. We then split the solution domain into the four asymptotic regimes illustrated in figure 6. In the *film region*, the base of the cell is firmly attached to the wall by adhesion molecules and $h \approx 1$. The curvature of the cell membrane in this region is small, so that the spring term dominates in (2.14). In the *corner region*, the membrane curvature is large, and the spring term and curvature term in (2.14) balance over a lengthscale $O(M^{-1/2})$. In the *bending region*, which is present when the corner moves sufficiently rapidly, the adhesion molecules have become disconnected and viscous stresses compete with membrane tension, and the membrane can exhibit a characteristic bulge. In the *outer region* the membrane is quadratic and in static equilibrium, which matches to the circular cell shape far from the wall.

Let the contact length between cell and wall be given by $x_0(t)$, where an explicit definition of x_0 will be given later, but where we assume for now that $x_0(t) \approx x_{\min}(t)$. We define the spreading speed as

$$V(x_0) = x_{0t} \tag{3.2}$$

and make a quasi-steady travelling-wave approximation, so that in the corner region $h(x,t) = h(z)$ where $z = M^{1/2}(x - x_0)$ and $x = x_0(t)$. Equation (2.14) becomes

$$\frac{V}{M^{3/2}}(1-h) - \frac{h^3}{12}\left(\frac{(h-1)}{\exp(\frac{1}{2}\gamma(h-1)^2)} - h_{zz}\right)_z = 0, \tag{3.3}$$

taking $h \sim 1$ to leading order as $z \to -\infty$. Assuming $V \ll M^{3/2}$, we can solve (3.3) using a perturbation expansion of the form

$$h(z) = h_0(z) + \frac{V}{M^{3/2}}h_1(z) + o\left(\frac{V}{M^{3/2}}\right). \tag{3.4}$$

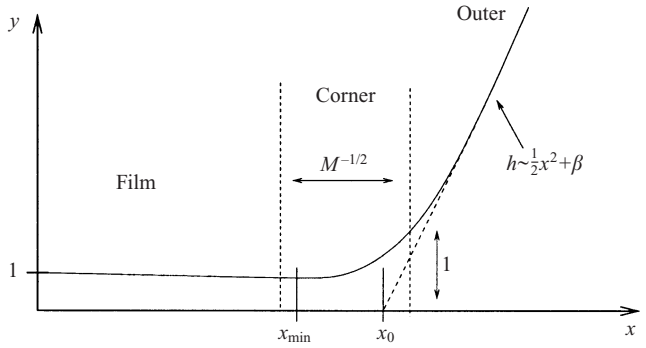

FIGURE 7. Schematic diagram of the three inner regions during slow spreading.

The leading-order term $h_0(z)$ is exactly the static corner solution discussed in § 2.3, for which $h_0 \sim (2/\gamma)^{1/2}z + A_0/\gamma^{-1/2} + 1$ as $z \to \infty$, where a numerical solution indicates that $A_0 \approx 0.626$ (consistent with (2.9)). Including the linear problem for h_1, we find

$$h \sim 1 + \frac{\mathrm{e}^z}{\gamma} + \frac{V}{M^{3/2}}\left(c + \frac{6z\mathrm{e}^z}{\gamma} + c_0\mathrm{e}^z\right) + \ldots \quad \text{as} \quad z \to -\infty, \tag{3.5}$$

where c and c_0 are constants. The $c_0\mathrm{e}^z$ term arises from an eigensolution of the homogeneous problem for h_1 that is proportional to $h_0'(z)$; c will be determined below. It follows that the leading-order depth of the fluid film laid down behind the moving corner in the film region (figure 6) h_F, and the corresponding pressure p_F, are

$$h_F(x) \sim 1 + cV(x)/M^{3/2}, \quad p_F \sim cV(x)/M^{1/2} \quad (0 < x < x_c), \tag{3.6}$$

where $V(x)$ is the speed of the corner when it passed station x (a relation determined below).

The general behaviour of h_0 and h_1 for large z is given by

$$h \sim \sqrt{\frac{2}{\gamma}}z + \frac{A_0}{\sqrt{\gamma}} + 1 + \frac{V}{M^{3/2}}(B_2z^2 - 6\gamma z\log z + B_1z) + \ldots \quad (z \to \infty), \tag{3.7}$$

for constants B_1 and B_2, where $B_2 = c_1 - (c/2)$ for some constant c_1 (c_1 arises from a contribution from the particular integral for h_1, and c multiplies a second eigenfunction of the homogeneous problem). For $\gamma = 1$, we find numerically that $c_1 \approx 4.021$.

We now consider two alternatives: rapid initial spreading, and slower spreading as the corner approaches its equilibrium position. Since slower spreading is simpler, we consider that case first.

3.2.1. *Slow later spreading*

When x_0 is close to its equilibrium location $x_c = (2M/\gamma)^{1/2}$, we match the corner region directly to the outer region (neglecting the bending region in figure 6), as sketched in figure 7. We first write the outer solution as

$$h \sim \tfrac{1}{2}x^2 + \beta = \tfrac{1}{2}(x - x_0)^2 + x_0(x - x_0) + \tfrac{1}{2}x_0^2 + \beta. \tag{3.8}$$

To formally match the quadratic term in (3.8) with that in (3.7), we set $V = M^{1/2}\tilde{V}$, where $\tilde{V} = O(1)$, and also write, for $M \gg 1$,

$$x_0 = \left(\frac{2M}{\gamma}\right)^{1/2} + x_1\frac{\log M}{M^{1/2}} + \frac{x_2}{M^{1/2}} + \ldots, \quad \beta = -\frac{M}{\gamma} + \beta_1 \log M + \beta_2 + \ldots. \tag{3.9}$$

To leading order, $h \sim x_0(x - x_0)$ when $x - x_0 = O(1)$ (making x_0 the effective contact angle); the dominant terms in (3.3) here are given by the widely studied equation often named after Tanner (1979; see also Duffy & Wilson 1997)

$$-Vh + \frac{h^3 h_{xxx}}{12} = 0 \tag{3.10}$$

(written in terms of x), which describes the competition between the effects of the wall moving with respect to the membrane and membrane tension. Using (3.10) we find that, with the first viscous correction,

$$h \sim \tfrac{1}{2}(x - x_0)^2 + x_0(x - x_0) + \tfrac{1}{2}x_0^2 + \beta - \frac{12V}{x_0^2}(x - x_0)\log(x - x_0) \tag{3.11}$$

in the inner limit of the outer region. Matching to (3.7) using intermediate variables (Van Dyke 1975) gives

$$(2/\gamma)^{1/2}x_1 + \beta_1 = 0, \quad A_0\gamma^{-1/2} + 1 = \beta_2 + x_2, \quad B_2\tilde{V} = \tfrac{1}{2}, \quad x_1 = -3\gamma\tilde{V}, \tag{3.12}$$

so that

$$x_0(V) = \left(\frac{2M}{\gamma}\right)^{1/2} - \frac{3\gamma V \log M}{M} + O(M^{-1/2}), \tag{3.13}$$

$$\beta(V) = -\frac{M}{\gamma} + 3V\log M\left(\frac{2\gamma}{M}\right)^{1/2} + O(1). \tag{3.14}$$

Equation (3.13) is effectively a linear relation between the effective contact angle x_0 and the contact-line speed, which with (3.14) can be integrated with respect to time (using 3.2) to obtain

$$x_0(t) = \left(\frac{2M}{\gamma}\right)^{1/2} - \exp\left[-\frac{M(t - t_0)}{3\gamma\log M}\right], \tag{3.15}$$

$$\beta(t) = -\frac{M}{\gamma} + \left(\frac{2M}{\gamma}\right)^{1/2}\exp\left[-\frac{M(t - t_0)}{3\gamma\log M}\right] \tag{3.16}$$

for some t_0. Notice that $x_0 \to (2M/\gamma)^{1/2}$ and $\beta \to -M/\gamma$ as $t \to \infty$, in agreement with the asymptotic static results (2.11), (2.12) for $k = 0$. Comparisons between (3.15), (3.16) and numerical results are presented in § 3.2.3 below.

3.2.2. *Rapid initial spreading*

Equation (3.13) suggests that earlier in spreading, when x_0 is far from its equilibrium point, the speed of the corner is

$$V = \frac{M^{3/2}}{\log M}\hat{V}, \tag{3.17}$$

for some $\hat{V} = O(1)$, so that the expansion in (3.4) is effectively in powers of $(\log M)^{-1}$. We now solve for h_1 assuming $B_2 = 0$ in (3.7), so that $c \approx 8.042$ for $\gamma = 1$. Even

without the quadratic term, (3.7) exhibits a non-uniformity for sufficiently large z, indicating that a new physical balance must be considered here.

For large z (and large h), the dominant balance of terms in (3.3) is (3.10), which occurs in the bending region (figure 6), between the corner and outer regions. To capture the way in which viscous forces cause a weak variation in membrane slope, we write

$$h = M^{1/2}(x - x_0)f(\zeta), \quad \zeta = \frac{\log(x - x_0)}{\log M}, \tag{3.18}$$

and then (3.10) becomes

$$f^2\left(\frac{f_{\zeta\zeta\zeta}}{(\log M)^2} - f_\zeta\right) = 12\hat{V}. \tag{3.19}$$

Thus, with error $O(1/(\log M)^2)$, $f^2 f_\zeta = -12\hat{V}$, so that

$$f = [36\hat{V}(\zeta_0 - \zeta)]^{1/3} \tag{3.20}$$

for some ζ_0. The outer limit of the corner solution (3.7), expressed in terms of f and ζ, becomes

$$f \sim (2/\gamma)^{1/2} - 6\gamma\hat{V}(\zeta + \tfrac{1}{2}) + \ldots \quad (\zeta \to -\tfrac{1}{2}). \tag{3.21}$$

We therefore set $\zeta_0 = -\frac{1}{2} + (2/\gamma)^{3/2}/(36\hat{V})$, ensuring continuity of f and f_ζ across $\zeta = -\frac{1}{2}$, giving

$$f(\zeta) = [(2/\gamma)^{3/2} - (\zeta + \tfrac{1}{2})(36\hat{V})]^{1/3}. \tag{3.22}$$

Note that while (3.10) suggests that membrane slopes might fall to $O(V^{1/3})$ across the bending region, i.e. to $O(M^{1/2}/(\log M)^{1/3})$, (3.22) (which must remain positive) indicates that the membrane slope remains $O(M^{1/2})$ here.

We suppose that the bending region matches onto the outer solution when $\log(x - x_0) = (\log M)^\upsilon$ for some $0 < \upsilon < 1$; at the boundary, where $\zeta \approx 1/(\log M)^{1-\upsilon}$, this gives a slope

$$f \sim [(2/\gamma)^{3/2} - 18\hat{V}]^{1/3} \tag{3.23}$$

to leading order in $(\log M)^{\upsilon-1}$, which matches to the slope x_0 in (3.8). Setting $\beta = -\frac{1}{2}x_0^2$, we obtain

$$x_0(V) = [(2M/\gamma)^{3/2} - 18V\log M]^{1/3}, \tag{3.24}$$

$$\beta(V) = -\frac{M}{\gamma}\left[1 - \frac{18V\log M}{(2M/\gamma)^{3/2}}\right]^{2/3}. \tag{3.25}$$

As the corner reaches an $O(1)$ distance from its equilibrium location, $\hat{V}$ falls and linearization of (3.24), (3.25) for $\hat{V} \ll 1$ yields (3.13), (3.14). At earlier times, when spreading is more rapid, the neglected terms involving powers of $1/\log M$ will be appreciable unless M is extremely large in magnitude. Below, we test the accuracy of (3.24), (3.25) against numerical solutions of the full problem.

The shape of the film deposited behind the moving corner is given by (3.6), i.e.

$$h = 1 + \frac{c}{M^{3/2}}\left[\frac{(2M/\gamma)^{3/2} - x^3}{18\log M}\right]. \tag{3.26}$$

This is consistent with the pressure distribution behind the advancing corner in figure 3(b). There is an analogy here with the thickness of a film depoisted behind an advancing meniscus (Landau & Levich 1942; Bretherton 1961); in that case also, a

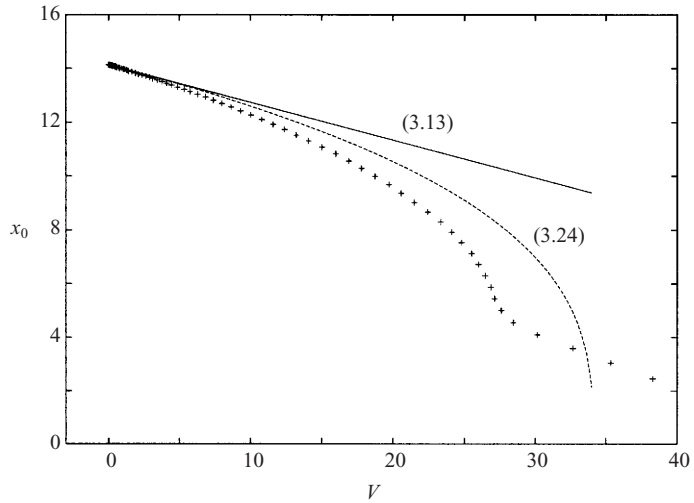

FIGURE 8. Symbols show corner position $x_0 \approx x_{\min} + 0.55$ (which is also the effective dynamic contact angle) computed numerically for $M = 100$, $\gamma = 1$ versus corner speed $V = \mathrm{d}x_{\min}/\mathrm{d}t$. Also shown are (3.24) (dashed) and (3.13) (solid).

faster-moving meniscus deposits a thicker film. Equation (3.26) can be used to provide an initial condition for (3.1) in the subsequent draining regime.

3.2.3. *Comparison with numerical solutions*

The symbols in figure 8 show numerical estimates of the relation between x_0 and V. Since $x_{\min} \approx x_c - 0.55$ at the end of the spreading phase, we plot $x_{\min} + 0.55$ to give a numerical estimate of x_0, and take $V \approx \mathrm{d}x_{\min}/\mathrm{d}t$. Also shown are predictions of x_0 versus V given by (3.13) (the linear relation for small V) and (3.24). All three results agree well for small V. The cubic behaviour in (3.24) is evident in the numerical data for large V; the asymptotics capture the qualitative behaviour well. The figure clearly demonstrates that viscous bending of the membrane is a significant effect in cell spreading, causing the effective contact angle x_0 to fall nonlinearly with increased spreading speed.

The rate of cell spreading can be found parametrically by solving (3.2) and (3.24). With $M = 100$ and $\gamma = 1$, (3.24), (3.25) imply $x_0 = 0$ and $\beta = 0$ when $V \approx 34.121$. We integrated from this point at $t = t_0$, choosing $t_0 = 1.1$ to give reasonable fit to the numerical solutions. The asymptotic predictions of $x_0(t)$ and $\beta(t)$ using (3.2), (3.24), (3.25) are plotted as dashed lines in figures 9 and 4(a) above, with symbols showing corresponding numerical solutions. Again we use $x_{\min} + 0.55$ as a numerical approximation of x_0. Also shown in each figure is the corresponding exponential relation (3.15), (3.16). As expected, the exponentials are accurate at late times, while the nonlinear relations (3.24), (3.25) extend the agreement at early times.

Given that the error in the asymptotic model is larger than $O(1/\log M) \approx 0.2$ early in spreading, falling to $O(1/M)$ at late times, agreement between numerics and asymptotics is very satisfactory. The asymptotics highlight the effects of trapped fluid ahead of the advancing corner: spreading rates are limited by the rate at which this fluid can be squeezed out of the shrinking gap between the cell and the wall; high fluid pressures cause bending of the membrane sufficient to produce a nonlinear relation between effective contact angle and the contact line speed. Only late in spreading, when the corner is near its equilibrium, is the angle–speed relation linear.

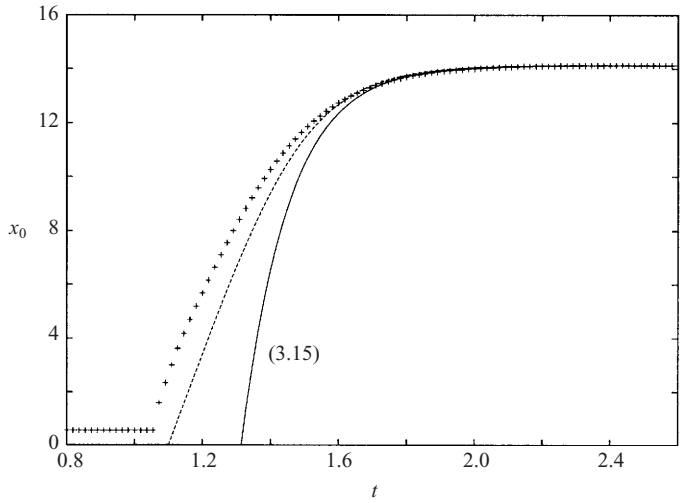

FIGURE 9. Symbols show $x_0 \approx x_{\min}(t) + 0.55$ versus time for $M = 100$, $\gamma = 1$ taken from the numerical solution of (2.14), (2.15). The dashed line shows $x_0(t)$ obtained from (3.2), (3.25); the solid line shows (3.15).

4. Aspiration off an adhesive wall

We have seen how adhesive forces can pull a cell normally onto a wall, so that ultimately it takes up a static configuration with a flat base (in $0 \leqslant x < x_c = (2M/\gamma)^{1/2}$, where $h = 1$), connected by a short transition region of width $O(M^{-1/2})$ to an outer region in which the cell is circular, such that the effective contact angle where the circular part of the cell meets the wall is $(2M/\gamma)^{1/2}$ (in (x, h) variables). We now examine the reverse process, in which a point force is applied to the top of the cell, pulling it vertically upwards from the wall. This is modelled using (2.14), (2.15) with $k > 0$, taking the $k = 0$ equilibrium configuration as an initial condition. Numerical results are presented in § 4.1. We will show in § 4.2 that much of the aspiration process can be understood using a quasi-steady asymptotic peeling analysis.

4.1. *Numerical results*

As in § 3.1, we illustrate aspiration of a cell off an adhesive wall with $M = 100$ and $\gamma = 1$. We solve (2.14), (2.15) numerically, ramping up k so that it is proportional to $\frac{1}{2}(1 - \cos(\pi t/t_r))$ for $0 \leqslant t < t_r = 0.2$, and then held constant thereafter. The critical value of k for complete removal of the cell from the wall is $k = \sqrt{2M/\gamma} \approx 14.14$, so setting $k = 15$ we expect the cell to leave the wall completely in finite time.

Figure 10 shows $h(x, t)$ and $p(x, t)$ during aspiration for $k = 15$. As soon as the point force is applied to the cell tip, the effective contact gradient between cell and wall is raised, leading to a marked increase in membrane curvature in the corner region, and correspondingly a locally low film pressure. The low pressure provides a dynamic adhesive force, and is typical of peeling motions (McEwan & Taylor 1966; Jensen *et al.* 2002). Figure 11 shows the position of the corner in the membrane during aspiration. The corner region propagates towards $x = 0$, with its propagation speed falling with time. If $k < (2M/\gamma)^{1/2}$, the corner comes to rest at its appropriate equilibrium location $x_c = (2M/\gamma)^{1/2} - k$. For the example with $k = 15$, the corner reaches $x = 0$ once $t \approx 0.55$; thereafter the cell is removed from the wall. Figure 12 shows the height of the cell centre D_c above the wall versus time,

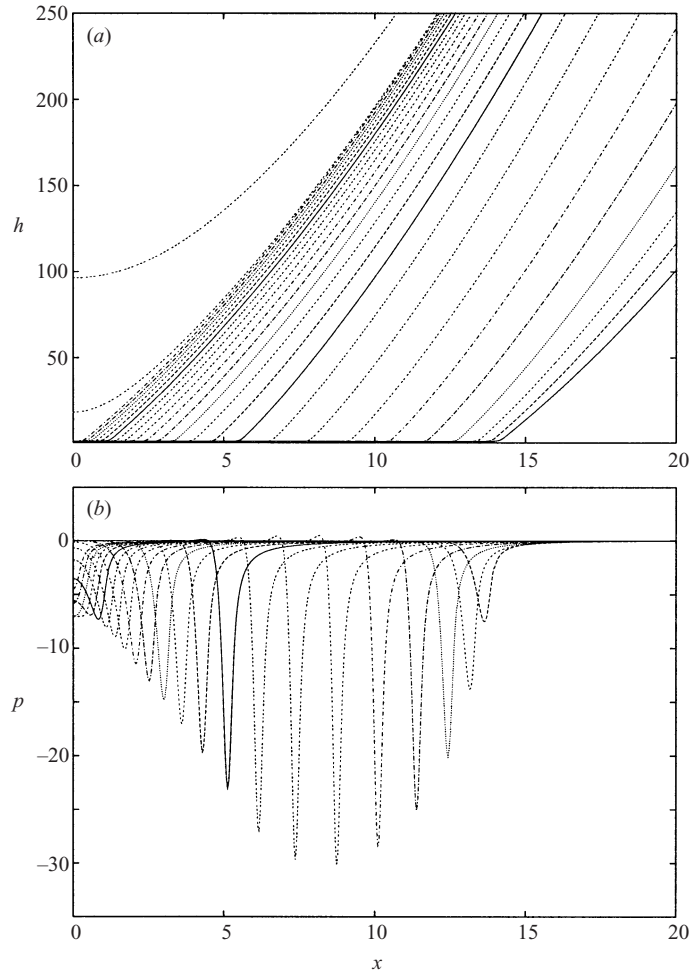

FIGURE 10. Solutions of (2.14), (2.15) with $M = 100$, $\gamma = 1$ and $k = 15$, showing (a) film depth and (b) pressure. At $t = 0$ the membrane is in equilibrium and $p = 0$ (solid). Subsequent solutions have time increments of 0.02; the cell membrane moves from right to left with time.

where D_c is given by

$$D_c(t) = r\cos(k\epsilon^{1/2}) + \epsilon\beta(t)$$
$$= 1 + 2k\epsilon^{1/2}/\pi - 25k^2\epsilon/4\pi - k^2\epsilon/2 + \epsilon\beta(t) + o(\epsilon), \tag{4.1}$$

assuming $1 \ll M \ll \epsilon^{-1/3}$. The cell centre rises sharply away from the wall as k is ramped up (for $0 \leqslant t < 0.2$, not shown fully in figure 12) and then then moves more slowly while the peeling is completed. For $k > (2M/\gamma)^{1/2}$ the cell then rises abruptly once more (at $t \approx 0.54$ for $k = 15$) as it detaches from the wall; for lower values of k the cell approaches a new equilibrium position. (We have illustrated this result with very small values of ϵ, to ensure the expression for D_c in (4.1) is strictly asymptotic.)

4.2. *Peeling asymptotics*

We seek here to capture as far as possible the results presented in figures 10–12 using a quasi-steady asymptotic peeling analysis, following closely the results presented in

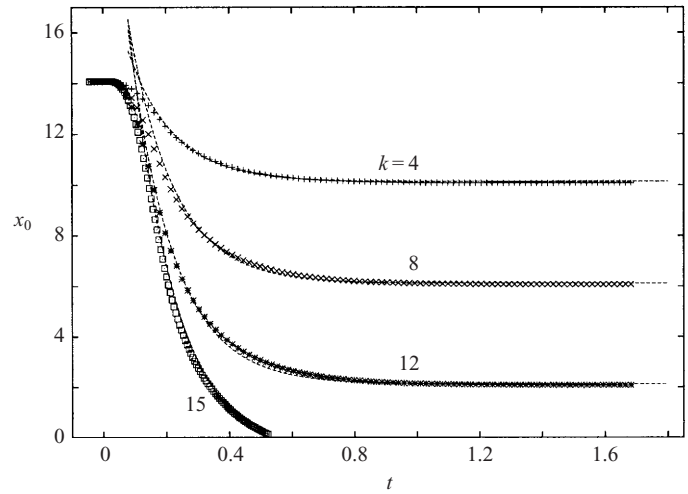

FIGURE 11. Lines show $x_0(t)$ given by (4.4) for $M = 100$, $\gamma = 1$ and $k = 4, 8, 12, 15$. The symbols are corresponding data from the numerical solution of (2.14), (2.15), taking $x_0 \approx x_{\min}$.

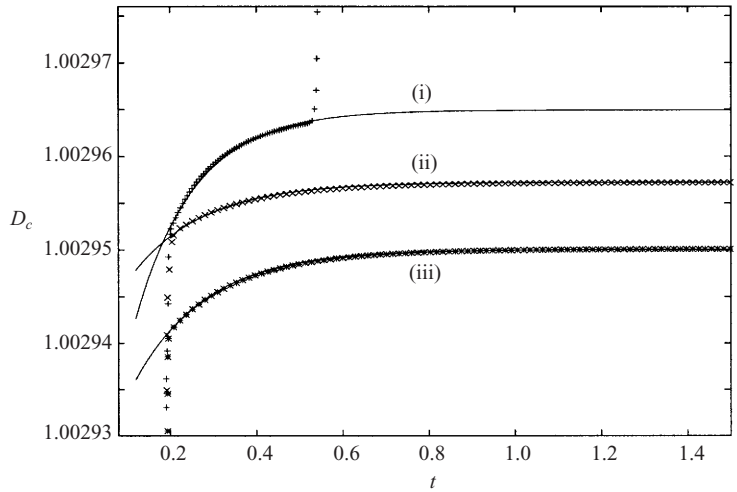

FIGURE 12. Symbols show $D_c(t)$ (the height of the centre of the cell above the plane) obtained from the numerical solution of (2.14). Parameter values are $M = 100$, $\gamma = 1$ and $(k, \epsilon) =$ (i) $(15, 1 \times 10^{-7})$, (ii) $(12, 1.56 \times 10^{-7})$, (iii) $(8, 3.54 \times 10^{-7})$ with k ramped up for $0 \leqslant t < 0.2$. Solid lines show $D_c(t)$ from (4.1) with $\beta(t)$ from (4.5) for the same parameter values but with k constant.

§ 3.2. For the parameter values illustrated here, it is sufficient to consider the low-speed, three-region asymptotic problem described in § 3.2.1 and sketched in figure 7.

The shape of the cell membrane in the quadratic outer region (figure 7) is

$$h(x) \sim \tfrac{1}{2}x^2 + kx + \beta = \tfrac{1}{2}(x - x_0)^2 + \phi(x - x_0) + (\beta + kx_0 + \tfrac{1}{2}x_0^2), \qquad (4.2)$$

where $\phi = x_0 + k$ is the effective contact angle that the outer solution makes with the wall at $x = x_0$. We define the peeling speed as $V = x_{0t}(t) < 0$, as in (3.2). Introducing a corner region around $x = x_0$ with $z = \sqrt{M}(x - x_0) = O(1)$, we obtain (3.3) once

again. Matching the outer limit (3.7) of the expansion (3.4) to (4.2), we find

$$\frac{VB_2}{M^{1/2}} = \frac{1}{2}, \quad \phi = x_0 + k = \left(\frac{2M}{\gamma}\right)^{1/2} - \frac{3\gamma V \log M}{M}, \quad \beta = -kx_0 - \tfrac{1}{2}x_0^2. \qquad (4.3a\text{–}c)$$

Equation (4.3*b*) shows how the dynamic contact angle increases with peeling speed (recall that $V < 0$). If $k < (2M/\gamma)^{1/2}$, so that the cell comes to a new equilibrium, then (4.3) with $V = 0$ predicts a static contact angle and contact length $\phi = \sqrt{2M/\gamma}$ and $x_0 = \sqrt{2M/\gamma} - k$ respectively, consistent with the static analysis in § 2.3. From (3.2), we can integrate (4.3*b*) with respect to time, yielding

$$x_0(t) = \left(\frac{2M}{\gamma}\right)^{1/2} - k + \exp\left[-\frac{M(t-t_0)}{3\gamma \log M}\right], \qquad (4.4)$$

$$\beta(t) = -\frac{M}{\gamma} + \frac{k^2}{2} - \left(\frac{2M}{\gamma}\right)^{1/2} \exp\left[\frac{-M(t-t_0)}{3\gamma \log M}\right] - \frac{1}{2}\exp\left[\frac{2M(t_0-t)}{3\gamma \log M}\right]. \qquad (4.5)$$

Figure 11 plots (4.4) as lines for $M = 100$, $\gamma = 1$ and $k = 4, 8, 12, 15$ to give a comparison with the numerical data from the solution to (2.14). The constant of integration t_0 is chosen in each case so that the expression given in (4.4) agrees with the numerical data at $t = 0.3$. After short initial transients, the overall agreement between numerics and asymptotics is excellent. Figure 12 shows (4.5) in (4.1) with k constant to give a comparison of D_c with the numerical data. The initial movement of the cell centre away from the wall is not captured since we have not ramped k, but once the full force is applied to the cell tip (4.5) captures the motion of the cell centre well. As $t \to \infty$, (4.5) predicts $\beta \to -M/\gamma + k^2/2$, as required by (2.12) and (4.1).

5. Cell rolling

We have demonstrated how cell sedimentation onto an adhesive wall, and aspiration off it, are dominated by quasi-steady spreading and peeling motions respectively. We show now how these motions also arise naturally when a two-dimensional cell tank-treads slowly along an adhesive wall in an external shear flow. This enables us to derive a relation between rolling speed and imposed shear rate as a function of M and γ.

We consider the configuration illustrated in figure 13. We again assume that $\epsilon \ll \epsilon M/\gamma \ll 1$, so that (as in figure 1*b*) the cell is almost circular away from the wall, and is in close contact with the wall over a short region of dimensional length $\epsilon^{1/2}LR = O(R(\epsilon M/\gamma)^{1/2}) \ll R$, where R is the cell radius. We suppose that the cell is exposed to a (dimensional) shear flow with velocity $(GY^\star, 0)$ where $\mu GR/\tau \ll 1$, so that the membrane tension is sufficiently strong compared to the imposed shear for the cell to remain nearly circular on lengthscales comparable to R. On these lengthscales, the cell resembles a rigid cylinder of radius R lying on a plane wall. Such a cylinder experiences a force per unit length parallel to the wall of $F^\star = 4\pi\mu RG$ (Schubert 1967; Davis & O'Neill 1977).

This force tilts the cell forwards slightly in the direction of the flow, decreasing the effective advancing contact angle $\epsilon^{1/2}\Theta^-$ and increasing the effective receding contant angle $\epsilon^{1/2}\Theta^+$ (figure 13) from their equilibrium values $\Theta^\pm = (2M/\gamma)^{1/2}$. The cell is assumed to roll (tank-tread) slowly and steadily over the wall at some speed $V^\star = (\tau\epsilon^{3/2}/\mu)V$, with spreading and peeling taking place at the front and rear of the cell respectively. We seek V in terms of M, γ and $F^\star$.

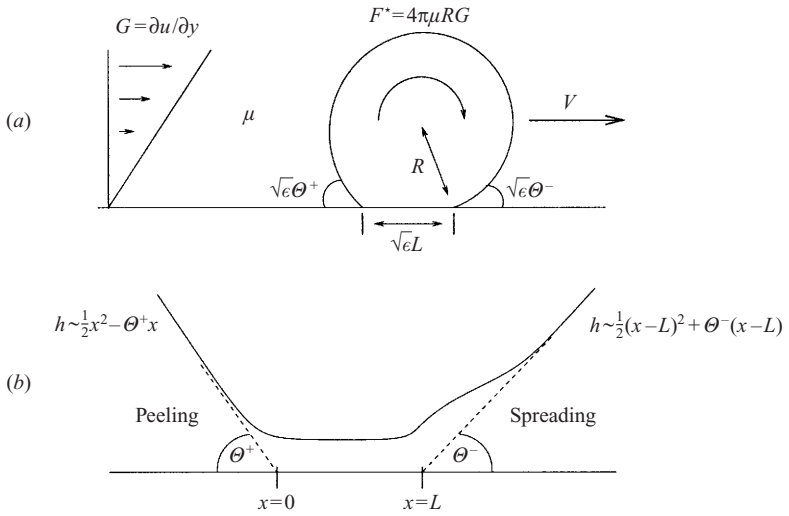

FIGURE 13. Schematic diagram of the outer (a) and inner (b) regions of a rolling cell.

In the presence of shear, a horizontal force balance on the cell requires

$$F^\star = \tau(\cos(\epsilon^{1/2}\Theta^-) - \cos(\epsilon^{1/2}\Theta^+)). \tag{5.1}$$

Here membrane tension acting in slightly different directions at the effective contact lines balances the hydrodynamic drag on the cell. Writing $F^\star = \epsilon\tau F$, (5.1) becomes

$$F = \tfrac{1}{2}(\Theta^{+2} - \Theta^{-2}) \tag{5.2}$$

with error $O(\epsilon)$. Away from the wall the cell is largely circular with radius $r = 1+O((\epsilon M/\gamma)^{3/2})$ (see § 2.3), so the geometrical relation $\sqrt{\epsilon}L = r\sin\sqrt{\epsilon}\Theta^- + r\sin\sqrt{\epsilon}\Theta^+$ implies

$$L = \Theta^- + \Theta^+ \tag{5.3}$$

with error $O(\epsilon, (\epsilon M/\gamma)^{3/2})$. We introduce the coordinate $\epsilon^{1/2}x$ along the wall, and write the gap between the cell and the wall as $\epsilon h(x)$. Then, as illustrated in figure 13(b), the inner limits of the outer circular solution can be written

$$h \sim \tfrac{1}{2}x^2 - \Theta^+ x \quad (x \to -\infty) \tag{5.4}$$

and

$$h \sim \tfrac{1}{2}(x-L)^2 + \Theta^-(x-L) \quad (x \to \infty). \tag{5.5}$$

With $z = x - L + \Theta^-$, (5.5) becomes $h \sim \frac{1}{2}z^2 - \frac{1}{2}\Theta^{-2}$ for $z \to \infty$, exactly the boundary condition used in spreading, (3.8). We can then exploit the spreading and peeling analyses of § 3.2 and § 4.2, relying on the nonlinear relation between contact angle and contact line speed (3.13) with $\alpha = 0$, so that the front and rear contact angles are

$$\Theta^\pm = [(2M/\gamma)^{3/2} \pm 18(\log M)V]^{1/3}, \tag{5.6}$$

from which F is obtained using (5.2). This relation can be simplified by setting $(\Theta^-, \Theta^+, L) = (2M/\gamma)^{1/2}(\bar\Theta^-, \bar\Theta^+, \bar L)$, $F = (M/\gamma)\bar F$, $V = ((2M/\gamma)^{3/2}/18\log M)\bar V$, so that

$$\bar\Theta^\pm = (1 \pm \bar V)^{1/3} \tag{5.7}$$

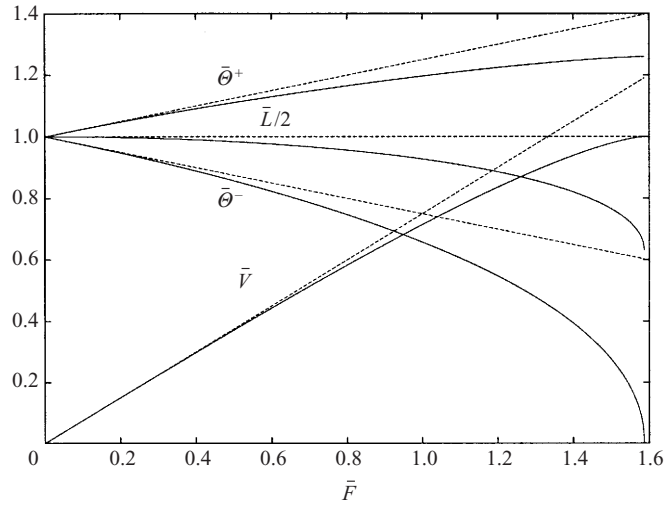

FIGURE 14. Scaled rolling velocity ($\bar{V}$), front and rear contact angles ($\bar{\Theta}^-$, $\bar{\Theta}^+$) and half contact length ($\bar{L}/2$) as fuctions of scaled force on cell $\bar{F}$. Solid lines show nonlinear relations (5.7), (5.8), dashed lines show linearized relations (5.9).

and

$$\bar{F} = (1+\bar{V})^{2/3} - (1-\bar{V})^{2/3}, \quad \bar{L} = (1+\bar{V})^{1/3} + (1-\bar{V})^{2/3}. \tag{5.8}$$

These relations are shown as solid lines in figure 14, alongside their linearized forms for $\bar{V} \ll 1$, for which

$$\bar{\Theta}^{\pm} \approx 1 \pm \tfrac{1}{3}\bar{V}, \quad \bar{F} \approx \tfrac{4}{3}\bar{V}, \quad \bar{L} \approx 2. \tag{5.9}$$

These relations represent the case in which viscous forces cause only weak bending of the membrane outside each contact line.

Figure 14 shows that at low speeds the rolling speed initially rises linearly with the imposed shear rate, but as the driving force increases, the front and rear contact angles (and the contact length) fall increasing rapidly, causing a plateau to develop in the speed–force relation. Once $\bar{F} = 2^{2/3}$, the front angle falls to zero; for larger shear rates the assumptions of the present approximation fail, and either a new form of steady structure emerges or else the steady solution terminates. Further implications of these results are discussed below.

6. Discussion and conclusions

We have presented here a continuum, deterministic model for a cell adhering to a plane surface. To keep the model tractable, numerous features of real cells (such as neutrophils) have been neglected. These include the bending stiffness of the cell membrane, cell membrane roughness (due to excess area stored as membrane folds, or due to microvilli), the effects of non-specific forces and non-uniform permeability of the cell–plane gap, arising for example due to the presence of glycocalyx, and the motion of bonds within the membrane. Particular weaknesses of the present model include the assumption of a two-dimensional rather than three-dimensional geometry, the assumption of equilibrium bond kinetics, and the neglect of the rheology of the cell interior, which would provide a viscoelastic resistance to spreading, peeling and rolling. The present model can be extended to incorporate these features. Binding mediated

stochastically by small numbers of individual bonds on the tips of individual microvilli is harder to capture within the present framework. Nevertheless, it is instructive to reflect on the predictions of the present model, both in terms of fundamental fluid mechanics and in terms of cell-adhesion applications.

Taking bond lengths to be substantially smaller than the cell radius ($\epsilon \ll 1$), we showed that macroscopic static cell configurations are governed (according to the present model) by the single parameter

$$\frac{\epsilon M}{\gamma} = \frac{F_a}{\tau}, \quad F_a = A_{tot} K_{eq} k_B T, \tag{6.1}$$

which measures the relative strength of the total adhesive force per unit length F_a (or adhesive energy density, Damiano *et al.* 1996) to membrane tension. For $\epsilon \ll (F_a/\tau) \ll 1$, the cell binds to the wall with a small but well-defined equilibrium contact angle

$$\theta_0 = (2F_a/\tau)^{1/2}, \tag{6.2}$$

consistent with the predictions of Evans (1985) and Dembo *et al.* (1988).

Using lubrication theory, we modelled sedimentation (§ 3), where adhesive forces pull an initially circular cell normally onto the wall. Initially a small segment of membrane is pulled rapidly onto the wall, displacing fluid sideways and causing the centre of the cell to be briefly lifted upwards (which we denote the *capture* phase, see figure 4). Then the width of the bound region increases until it reaches its equilibrium length (the *spreading* phase, figure 3), pulling the cell centre downwards and trapping a small amount of fluid between the bound membrane and the wall. Some of this fluid then drains slowly out from beneath the cell until the system is in complete equilibrium. Using an asymptotic analysis, taking $M \gg 1$, we found that the dimensionless spreading speed is $O((M/\gamma)^{3/2}/\log M)$, and that spreading occurs over a time of $O(\gamma(\log M)/M)$. Dimensionally, the adhesive timescale is

$$T_a = \frac{R\mu}{F_a} \log\left(\frac{\kappa A_{tot} K_{eq} R\lambda}{\tau}\right), \tag{6.3}$$

which is only weakly dependent on membrane tension, bond stiffness and bond length, but strongly dependent on fluid viscosity and bond density. T_a is controlled primarily by a ratio of viscous to adhesive forces, showing that the rate of spreading is controlled by the speed at which fluid can be squeezed out of the narrow gap between the cell and the plane. To model the reverse process (aspiration), a point force is applied to the top of a bound cell, pulling the cell off the wall (§ 4). Our analysis shows that the membrane peels away from the wall also over an $O(T_a)$ timescale, at least for forces just large enough to lead to complete cell detachment.

A key aspect of the asymptotic description of both spreading and peeling is the identification of a relationship between the effective contact angle θ of the cell (where the nearly circular outer solution approaches the wall), the speed $V^\star$ of the effective contact line and the equilibrium contact angle θ_0 (which is also the microscopic contact angle when the gap thickness is $O(\lambda)$). In dimensional terms, we find that (from (3.13))

$$\theta^3 \approx \theta_0^3 - 18\left(\frac{\mu V^\star}{\tau}\right) \log\left(\frac{\kappa A_{tot} K_{eq} R\lambda}{\tau}\right). \tag{6.4}$$

In spreading, $V^\star > 0$ and θ is reduced below its equilibrium value; in peeling $V^\star < 0$ and θ exceeds θ_0. In (6.4) we recognise $\mu V^\star/\tau \approx (F_a/\tau)^{3/2} \ll 1$ as a capillary number.

In spreading, fluid is trapped in the closing gap between the membrane and the wall: in being squeezed out of the gap, it elevates pressures and causes the membrane to bulge, lowering the effective contact angle according to (6.4). In peeling, fluid has to be sucked into the opening gap: the low fluid pressures cause the membrane to bend in the opposite direction. Equation (6.4) is typical of nonlinear relations between contact angle and contact line speed (Oron *et al.* 1997), and arises in a wide class of thin-film problems (King 2001), although it suffers from the usual weaknesses of asymptotics involving logarithmic corrections which in practical situations can have limited accuracy. As observed in pure fluid systems, the effective dynamic contact angle depends (albeit weakly) on the macroscopic dimensions of the cell (in contrast to θ_0, which is entirely determined by a local force balance).

By assuming that bond formation and breakage occur much more rapidly than the adhesive timescale T_a, so that binding is always in equilibrium, we cannot distinguish between the 'catch' and 'slip' bonds introduced by Dembo *et al.* (1988) (for which the unbinding rate of a bond either decreases or increases with applied force). Accounting for such effects, Dembo *et al.* obtained a relation between peeling speed, imposed tension and peeling angle. Future studies should examine how non-equilibrium kinetics and hydrodynamic forces (through (6.4)) together influence adhesion processes; their interaction has been incorporated only implicity in the existing computational models of Lei *et al.* (1999) and Dong *et al.* (1999).

An attractive feature of the present equilibrium assumption is that the binding forces can be represented as an adhesive potential which is long-range attractive, short-range repulsive, entering the model as an effective conjoining/disjoining pressure (see (2.13)). Aspects of the present analysis can therefore be carried over to problems involving hole growth in a rupturing liquid film (where a receding contact line corresponds to what we here call spreading) or problems with a driven advancing contact line (which we call peeling). The low fluid pressures ahead of the advancing corner in peeling suggest the possibility of a spanwise fingering instability (McEwan & Taylor 1966). As is well known from studies of thin liquid films subject to long-range van der Waals forces, an attractive potential can drive spontaneous long-wave instabilities leading to film rupture (Williams & Davis 1982; Oron *et al.* 1997). Equation (2.14) shares this property for initially uniform film thicknesses $h_0 > 1 + \gamma^{-1/2}$, for which $f'(h_0) < 0$, where $f(h) = M(h-1)\exp(-\frac{1}{2}\gamma(h-1)^2)$. Such instabilities have been recognized in the context of cell adhesion as a possible mechanism for sites of focal adhesion (Gallez & Coakley 1986; Ward & Hammer 1993; Gallez, De Wit & Kaufman 1996). Under boundary conditions (2.15), however, we found no evidence of such instabilities for the parameter values we investigated.

The relation (6.4) was used in § 5 to analyse the tank-treading rolling motion of a nearly circular cell adhering to a wall in a shear flow, when the rolling speed is determined by viscous dissipation in the suspending fluid. The shear force on the cell is balanced by membrane tension acting at the front and rear effective contact lines; the rear contact angle (where the membrane is peeling off the wall) is larger than the front contact angle (where the membrane is spreading onto the wall). For a low shear rate G (with $RG\mu \ll F_a \ll \tau$), so that each contact angle differs only marginally from θ_0, the dimensional rolling speed is (from (5.9))

$$V^\star = \frac{\pi RG}{3}\left(\frac{2F_a}{\tau}\right)^{1/2} \Big/ \log\left(\frac{\kappa A_{tot} K_{eq} R\lambda}{\tau}\right), \tag{6.5}$$

which is smaller than the free-stream speed RG by a factor comparable to the equilibrium contact angle θ_0. Surprisingly, (6.5) predicts that rolling speed increases

with increased adhesive force F_a. The explanation for this is that increasing F_a (subject of course to the constraint $F_a \ll \tau$) increases the equilibrium contact angle, increasing the mobility of the suspending fluid near each contact line and so increasing the mobility of the cell as a whole. Equation (6.5) is also independent of viscosity μ: increasing μ increases the drag on the cell but also increases the resistance to flow near the contact lines, and the two effects cancel. Whether this mechanism might explain a viscosity-independent rolling-speed/shear-rate relationship reported for rolling leukocytes (Smith *et al.* 2001) is at present being investigated. Independence of μ may be an artefact of the two-dimensional geometry, since in three dimensions fluid trapped near contact lines can escape sideways around the base of the cell as well as by moving parallel to the primary flow direction. Also, once $RG\mu = O(F_a)$ the nonlinearity in (6.4) becomes important, and the velocity–force relation (5.8) depends explicitly on μ (figure 14). Viscous effects reduce rolling speeds to beneath that predicted by (6.5), and suggest the existence of the plateau seen in velocity–force curves found experimentally (Atherton & Born 1973) and theoretically in other studies (Lei *et al.* 1999). However, once $V^\star$ is large enough for the advancing contact angle to reach zero according to (6.4), the assumed asymptotic structure breaks down. Kan *et al.* (1999) show how a long region of fluid can be trapped beneath the front of an adherent cell; our analysis may provide an estimate of when this behaviour first arises.

In a recent computational study, Dong *et al.* (1999) computed transient adhesion events for a model two-dimensional cell bound to a wall in a shear flow. They assumed that the net force on the cell is balanced by tensile forces in a short peeling zone at the cell's trailing edge. While the present study differs significantly from this one both in terms of the model and the parameter ranges investigated, there are important qualitative features common to both studies. Our model demonstrates, for example, that at low shear rates ($\mu RG \ll F_a$) high pressures in the suspending fluid where the front of the cell is spreading onto the plane can be just as important as low pressures in the peeling region in the overall force balance (and in practice these high pressures may be important in squashing glycocalyx immediately ahead of the advancing cell to expose ligand molecules), although the peeling region dominates the force balance once $\mu RG = O(F_a)$. Our approach also identifies the natural asymptotic structure of the 'peeling zone' postulated in the computational model, for membranes characterized by tension alone.

In summary, the present model shows how viscous forces in the suspending fluid can (in principle) limit the rate at which a cell spreads, peels and rolls over an adhesive surface. However to test definitively whether or not the hydrodynamical effects described are biologically significant requires further refinements of the model (accounting particularly for three-dimensionality, membrane bending forces, cytoplasmic rheology and nonequilibrium binding kinetics).

O. E. J. is indebted to Donald P. Gaver and David Halpern for invaluable discussions during the initial development of the model, and acknowledges enlightening conversations with John King and Klaus Ley. S. R. H. was supported by an EPSRC Studentship.

REFERENCES

Alon, R., Chen, S., Fuhlbrigge, R., Puri, K. D. & Springer, T. A. 1998 The kinetics and shear threshold of transient and rolling interactions of L-selectin with its ligand on leukocytes. *Proc. Natl Acad. Sci. USA* **95**, 11631–11636.

Atherton, A. & Born, G. V. R. 1973 Relationship between the velocity of rolling granulocytes and that of the blood flow in venules. *J. Physiol. Lond.* **233**, 157–165.

Bell, G. I. 1978 Models for the specific adhesion of cells to cells. *Science* **200**, 618–627.

Bongrand, P. 1999 Ligand-receptor interactions. *Rep. Prog. Phys.* **62**, 921–968.

Bretherton, F. P. 1961 The motion of long bubbles in tubes. *J. Fluid Mech.* **10**, 166–188.

Brooks, S. B. & Tözeren, A. 1996 Flow past an array of cells that are adherent to the bottom plate of a flow channel. *Comput. Fluids* **25**, 741–757.

Cantat, I. & Misbah, C. 1999 Lift force and dynamical unbinding of adhering vesicles under shear flow. *Phys. Rev. Lett.* **83**, 880–883.

Chang, K.-C. & Hammer, D. A. 1999 The forward rate of binding of surface-tethered reactants: effect of relative motion between two surfaces. *Biophys. J.* **76**, 1280–1292.

Chang, K.-C., Tees, D. F. J. & Hammer, D. A. 2000 The state diagram for cell adhesion under flow: leukocyte rolling and firm adhesion. *Proc. Natl Acad. Sci. USA* **97**, 11262–11267.

Chen, S. & Springer, T. A. 1999 An automatic braking system that stabilizes leukocyte rolling by an increase in selectin bond number with shear. *J. Cell Biol.* **144**, 185–200.

Chen, S. & Springer, T. A. 2001 Selectin receptor-ligand bonds: formation limited by shear rate and dissociation governed by the Bell model. *Proc. Natl Acad. Sci. USA* **98**, 950–955.

Damiano, E. R., Westheider, J., Tözeren, A. & Ley, K. 1996 Variation in the velocity, deformation, and adhesion energy density of leukocytes rolling within venules. *Circ. Res.* **79**, 1122–1130.

Davis, A. M. J. & O'Neill, M. E. 1977 Separation in a slow linear shear flow past a cylinder and a plane. *J. Fluid Mech.* **81**, 551–564.

Dembo, M., Torney, D. C., Saxman, K. & Hammer, D. A. 1988 The reaction-limited kinetics of membrane-to-surface adhesion and detachment. *Proc. R. Soc. Lond.* B **234**, 55–83.

Dimitrakopoulos, P. & Higdon, J. J. L. 1997 Displacement of fluid droplets from solid surfaces in low-Reynolds-number shear flows. *J. Fluid Mech.* **336**, 351–378.

Dong, C., Cao, J., Struble, E. J. & Lipowsky, H. H. 1999 Mechanics of leukocyte deformation and adhesion to endothelium in shear flow. *Ann. Biomed. Engng* **27**, 298–312.

Dong, C. & Lei, X. X. 2000 Biomechanics of cell rolling: shear flow, cell-surface adhesion, and cell deformability. *J. Biomech.* **33**, 35–43.

Duffy, B. R. & Wilson, S. K. 1997 A third-order differential equation arising in thin-film flows and relevant to Tanner's law. *Appl. Math. Lett.* **10**, 63–68.

Dussan V., E. B. 1987 On the ability of drops to stick to surfaces of solids. Part 3. The influences of the motion of the surrounding fluid on dislodging drops. *J. Fluid Mech.* **174**, 381–397.

Eres, M. H., Schwartz, L. W. & Roy, R. V. 2000 Fingering phenomena for driven coating films. *Phys. Fluids* **12**, 1278–1295.

Evans, E. 1985 Detailed mechanics of membrane-membrane adhesion and separation. *Biophys. J.* **48**, 175–183.

Evans, E. & Ritchie, K. 1997 Dynamic strength of molecular adhesion bonds. *Biophys. J.* **72**, 1541–1555.

Feng, J. Q. & Basaran, O. A. 1994 Shear flow over a translationally cylindrical bubble pinned on a slot in a plane wall. *J. Fluid Mech.* **275**, 351–378.

Feng, J. & Weinbaum, S. 2000 Lubrication theory in highly compressible porous media: the mechanics of skiing, from red cells to humans. *J. Fluid Mech.* **422**, 281–317.

Finger, E. B., Puri, K. D., Alon, R., Lawrence, M. B., von Andrian, U. H. & Springer, T. A. 1996 Adhesion through L-selectin requires a threshold hydrodynamic shear. *Nature* **379**, 266–269.

Gallez, D. & Coakley, W. T. 1986 Interfacial instability at cell membranes. *Prog. Biophys. Mol. Biol.* **48**, 155–199.

Gallez, D., De Wit, A. & Kaufman, N. 1996 Dynamics of a thin liquid-film with a surface chemical-reaction. *J. Colloid Interface Sci.* **180**, 524–536.

Gaver, D. P. III & Kute, S. M. 1998 A model study of the influence of fluid stresses on a cell adhering to a microchannel wall. *Biophys. J.* **75**, 721–733.

Goetz, D. J., El-Sabban, M. E., Pauli, B. U. & Hammer, D. A. 1994 Dynamics of neutrophil rolling over stimulated endothelium in vitro. *Biophys. J.* **66**, 2202–2209.

Goldman, A. J., Cox, R. G. & Brenner, H. 1967*a* Slow viscous motion of a sphere parallel to a plane wall – I. Motion through a quiescent fluid. *Chem. Engng Sci.* **22**, 637–651.

Goldman, A. J., Cox, R. G. & Brenner, H. 1967*b* Slow viscous motion of a sphere parallel to a plane wall – II. Couette flow. *Chem. Engng Sci.* **22**, 653–660.

Hammer, D. A. & Apte, S. M. 1992 Simulation of cell rolling and adhesion on surfaces in shear flow: general results and analysis of selectin-mediated neutrophil adhesion. *Biophys. J.* **63**, 35–57.

Hammer, D. A. & Lauffenburger, D. A. 1987 A dynamical model for receptor-mediated cell adhesion to surfaces. *Biophys. J.* **52**, 475–487.

Hammer, D. A. & Tirrell, M. 1996 Biological adhesion at interfaces. *Annu. Rev. Mater. Sci.* **26**, 651–691.

Hochmuth, R. M. 2000 Micropipette aspiration of living cells. *J. Biomech.* **33**, 15–22.

Jensen, O. E., Horsburgh, M. K., Halpern, D. & Gaver, D. P. III 2002 The steady propagation of a bubble in a flexible-walled channel: asymptotic and computational models. *Phys. Fluids* **14**, 443–457.

Jones, D. A., Smith, C. W. & McIntyre, L. V. 1996 Leucocyte adhesion under flow conditions: principles important in tissue engineering. *Biomaterials* **17**, 337–347.

Kan, H. C., Udaykumar, H. S., Shyy, W. & Tran-Son-Tay, R. 1999 Numerical analysis of the deformation of an adherent drop under shear flow. *J. Biomech. Engng* **121**, 160–169.

King, J. R. 2001 Thin-film flows and high-order degenerate parabolic equations. In *IUTAM Symposium on Free Surface Flows* (ed. Y. Shikmurzaev). Kluwer.

King, M. R. & Hammer, D. A. 2001 Multiparticle adhesive dynamics: interactions between stably rolling cells. *Biophys. J.* **81**, 799–813.

Landau, L. D. & Levich, B. 1942 Dragging of a liquid by a moving plate. *Acta Physicochim. USSR* **17**, 42–54.

Lauffenburger, D. A. & Linderman, J. J. 1993 *Receptors: Models for Binding, Trafficking and Signalling*. Oxford University Press.

Lawrence, M. B. 1999 Selectin-carbohydrate interactions in shear flow. *Curr. Opin. Chem. Biol.* **3**, 659–664.

Lawrence, M. B. & Springer, T. A. 1991 Leukocytes roll on a selectin at physiologic flow rates: distinction from and prerequisite for adhesion through integrins. *Cell* **65**, 859–873.

Leckband, D. 2000 Measuring the forces that control protein interactions. *Annu. Rev. Biophys. Biomol. Struct.* **29**, 1–26.

Lei, X., Lawrence, M. B. & Dong, C. 1999 Influence of cell deformation on leukocyte rolling adhesion in shear flow. *J. Biomech. Engng* **121**, 636–643.

Li, X. & Pozrikidis, C. 1996 Shear flow over a liquid drop adhering to a solid surface. *J. Fluid Mech.* **307**, 167–190.

McEwan, A. D. & Taylor, G. I. 1966 The peeling of a flexible strip attached by a viscous adhesive. *J. Fluid Mech.* **26**, 1–15.

Mitlin, V. S. 1993 Dewetting of solid surface: analogy with spinodal decomposition. *J. Colloid Interface Sci.* **156**, 491–497.

Olivier, L. A. & Truskey, G. A. 1993 A numerical analysis of forces exerted by laminar flow on spreading cells in a parallel plate flow chamber assay. *Biotech. Bioengng* **42**, 963–973.

Oron, A. 2000 Three-dimensional nonlinear dynamics of thin liquid films. *Phys. Rev. Lett.* **85**, 2108–2111.

Oron, A. Davis, S. H. & Bankoff, S. G. 1997 Long-scale evolution of thin liquid films. *Rev. Mod. Phys.*, **69**, 931–980.

Orsello, C. E., Lauffenburger, D. A. & Hammer, D. A. 2001 Molecular properties in cell adhesion: a physical and engineering perspective. *Trends Biotech.* **19**, 310–316.

Piper, J. W., Swerlick, R. A. & Zhu, C. 1998 Determining force dependence of two-dimensional receptor-ligand binding affinity by centrifugation. *Biophys. J.* **74**, 492–513.

Schleizer, A. D. & Bonnecaze, R. T. 1999 Displacement of a two-dimensional immiscible droplet adhering to a wall in shear and pressure-driven flows. *J. Fluid Mech.* **383**, 29–54.

Schubert, G. 1967 Viscous flow near a cusped corner. *J. Fluid Mech.* **27**, 647–656.

Seifert, U. 1991 Adhesion of vesicles in two dimensions. *Phys. Rev.* A **43**, 6803–6814.

Seifert, U. 1999 Hydrodynamic lift on bound vesicles. *Phys. Rev. Lett.* **83**, 876–879.

Seifert, U. & Lipowsky, R. 1990 Adhesion of vesicles. *Phys. Rev.* A **42**, 4768–4771.

Shao, J.-Y., Ting-Beall, H. P. & Hochmuth, R. M. 1998 Static and dynamic lengths of neutrophil microvilli. *Proc. Natl Acad. Sci.* **95**, 6797–6802.

Sharma, A. & Jameel, A. T. 1993 Nonlinear stability, rupture, and morphological phase separation of thin fluid films on apolar and polar substrates. *J. Colloid Interface Sci.* **161**, 190–208.

Sheik, S. & Nash, G. B. 1998 Treatment of neutrophils with cytocholasins converts rolling to stationary adhesion on P-selectin. *J. Cell Physiol.* **174**, 206–216.

Smith, M. J., Berg, E. L. & Lawrence, M. B. 1999 A direct comparison of selectin-mediated transient, adhesive events using high temporal resolution. *Biophys. J.* **77**, 3371–3383.

Smith, M. L., Smith, M. J., Lawrence, M. B. & Ley, K. F. 2001 Leukocyte rolling velocity is determined by wall shear rate, not wall shear stress. *FASEB J.* **15** A393.

Springer, T. A. 1995 Traffic signals on endothelium for lymphocyte recirculation and leukocyte emigration. *Annu. Rev. Physiol.* **57**, 827–872.

Sukumaran, S. & Seifert, U. 2001 Influence of shear flow on vesicles near a wall: a numerical study. *Phys. Rev.* E **64**, 011916-1–011916-11.

Tanner, L. H. 1979 The spreading of silicone oil drops on horizontal surfaces. *J. Phys.* D: *Appl. Phys.* **12**, 1473–1484.

Tissot, O., Pierres, A., Foa, C., Delaage, M. & Bongrand, P. 1992 Motion of cells sedimenting on a solid surface in a laminar shear flow. *Biophys. J.* **61**, 204–215.

Tözeren, A & Ley, K. 1992 How do selectins mediate leukocyte rolling in venules? *Biophys. J.* **63**, 700–709.

Van Dyke, M. 1975 *Perturbation Methods in Fluid Mechanics.* Parabolic Press, Stanford, California.

Ward, M. D., Dembo, M. & Hammer, D. A. 1995 Kinetics of cell detachment: effect of ligand density. *Ann. Biomed. Engng* **23**, 322–331.

Ward, M. D. & Hammer, D. A. 1993 Morphology of cell-substratum adhesion. *Cell Biophys.* **20**, 177–222.

Williams, M. B. & Davis, S. H. 1982 Nonlinear theory of film rupture. *J. Colloid Interface Sci.* **90**, 220–228.

Wu, S., Hoxter, B., Byers, S. W. & Tözeren, A. 1998 Role of cytoskeleton and deformability in laminin-mediated cell rolling. *Biorheology* **35**, 37–51.

Zhao, Y., Chien, S. & Weinbaum, S. 2001 Dynamic contact forces on leukocyte microvilli and their penetration of the endothelial glycocalyx. *Biophys. J.* **80**, 1124–1140.

Zhu, C. 2000 Kinetics and mechanics of cell adhesion. *J. Biomech.* **33**, 23–33.

Zhu, C., Bao, G. & Wang, N. 2000 Cell mechanics: mechanical response, cell adhesion and molecular deformation. *Annu. Rev. Biomed. Engng* **2**, 189–226.